Departament de Teoria
del Senyal i Comunicacions
UNIVERSITAT POLITÈCNICA DE CATALUNYA

MULTIDIMENSIONAL SPECKLE NOISE, MODELLING AND FILTERING RELATED TO SAR DATA

by

Carlos López Martínez

Xavier Fàbregas Cànovas, Thesis Advisor

Ph.D. Dissertation

Thesis Committee: Antoni Broquetas i Ibars
Ignasi Corbella i Sanahuja
Jong-Sen Lee
Eric Pottier
Juan Manuel López Sánchez

Barcelona, June 2, 2003

Chapter 4

Interferometric Phasor Noise Model

4.1 Introduction

As it has been evidenced in Chapter 2, SAR technology is an important tool to gather information concerning the Earth's surface. Depending on the SAR system configuration, collected data can be related with different surface's properties among which topography, soil moisture or vegetation height have a particular importance. This information is not directly contained within SAR data. As a consequence, inversion processes have to be designed for its extraction [36,165]. The inversion process has to deal with the inherent complexity of the electromagnetic scattering process. Electromagnetic scattering models have to be employed to extract the physical parameters of interest from the radar observables, as for instance the interferometric phase in the case of InSAR or the covariance matrix in PolSAR. Nevertheless, the estimation of these observables is not a trivial task due to the presence of speckle noise [7,166,167].

Speckle noise in SAR imagery is a major problem as it hinders obtaining relevant information. Section 2.1.6 at Chapter 2 showed that speckle noise can be modelled as a multiplicative noise term for the SAR image intensity. Within Section 2.2.5 at the same chapter, it was demonstrated that under proper conditions, speckle noise can be modelled as an additive noise component for the phase difference between a pair of correlated SAR images. On the contrary speckle noise models do not exist for multidimensional SAR imagery as PolSAR or PolInSAR.

This chapter concerns the definition of a new speckle noise model for the interferometric phase difference coded at the complex plane as a unit amplitude phasor. In addition, this model will be also derived within the transformed wavelet domain. The main reason behind the use of the wavelet theory for this problem is the possibility to estimate relevant interferometric information with a high spatial resolution. Furthermore, the theory presented in the following establishes a basis to define a general speckle noise model for multidimensional SAR data, as it will be presented at the next chapter.

In order to avoid confusion, whenever necessary, the imaginary number $\sqrt{-1}$ will be indicated as $\mathbf{j}$, whereas the wavelet scale will be denoted by 2^j.

4.2 Interferometric Phasor Noise Model

Speckle noise, for single SAR images, is modelled as a complex noise term with Rayleigh distributed amplitude and uniformly distributed phase. The main consequence of this model is that speckle noise has a multiplicative nature for the amplitude and an additive nature for the phase. However, the multiplicative

noise model can not be extended for those cases in which information is extracted from the combination of SAR images as InSAR, PolSAR and PolInSAR, since it prevents the use of the phase difference as a source of useful information.

It has been proved that the interferometric phase difference between two SAR images S_1 and S_2, under the assumption of Gaussian scattering, is described by the probability density function (pdf) given in Eq. (2.110). This pdf can be also derived as a marginal density from the multivariate complex Wishart distribution, whose general expression is given by Eq. (2.181). The interferometric phase distribution is a bell-shaped curve with its mode located at ϕ_x. Within the phase interval $[\phi_x - \pi, \phi_x + \pi)$, the interferometric phase noise can be modelled by an additive noise term [168, 94]

$$\phi = \phi_x + v \tag{4.1}$$

where ϕ represents the measured interferometric phase, ϕ_x denotes the true interferometric phase, and v is the signal independent additive noise component. However, the interferometric phase is only measured within the interval $[-\pi, \pi)$. Consequently, it is necessary to unwrap it in order to make use of the noise model given by Eq. (4.1) [94].

A different approach consists on defining a noise model in the complex plane, i.e., an interferometric phase noise model valid within the interval $[-\pi, \pi)$, independently of the position of the phase mode ϕ_x. In the complex plane, the measured interferometric phase ϕ can be expressed as the unit amplitude complex phasor

$$e^{j\phi} = \Re\{e^{j\phi}\} + j\Im\{e^{j\phi}\} = \cos(\phi) + j\sin(\phi)\,. \tag{4.2}$$

In the following, $e^{j\phi}$ is referred as the *measured interferometric phasor* or simply *interferometric phasor*, whereas $e^{j\phi_x}$ is called the *true interferometric phasor* [169]. Since the trigonometric functions $\cos(\cdot)$ and $\sin(\cdot)$ of the measured interferometric phase ϕ are periodic, it follows

$$\cos(\phi) = \cos(\phi_x + v) = \cos(\phi_x + v - 2\pi k) \quad \forall k \in \mathbb{Z} \tag{4.3}$$

$$\sin(\phi) = \sin(\phi_x + v) = \sin(\phi_x + v - 2\pi k) \quad \forall k \in \mathbb{Z}. \tag{4.4}$$

This makes possible to consider the additive interferometric phase noise model in the interval $[-\pi, \pi)$, provided the phase ϕ to be the argument of $\cos(\cdot)$ or $\sin(\cdot)$. The rest of this section concerns the definition of a interferometric phasor noise model.

Using the formulas for the addition and difference of angles with trigonometric functions, the real and imaginary parts of the interferometric phasor can be decomposed as

$$\cos(\phi) = \cos(\phi_x)\cos(v) - \sin(\phi_x)\sin(v) \tag{4.5}$$

$$\sin(\phi) = \cos(\phi_x)\sin(v) + \sin(\phi_x)\cos(v). \tag{4.6}$$

As it can be observed, the true interferometric phase ϕ_x has been separated from the noise term v. Therefore, the noise term v can be considered as being distributed according to Eq. (2.110), assuming $\phi_x = 0$ rad. If the useful signal ϕ_x, as well as the phase noise v are considered homogeneous, the terms $\cos(\phi_x)$ and $\sin(\phi_x)$ can be assumed to be constant values, whereas $\cos(v)$ and $\sin(v)$ are homogeneous random processes.

The noise terms in the complex plane, defined as $v_1 = \cos(v)$ and $v_2 = \sin(v)$, are described by the following pdfs

$$p_{v_1}(v_1) = \frac{1}{\pi\sqrt{1-v_1^2}} \frac{\left(1-|\rho|^2\right)\left[\left(1-|\rho|^2 v_1^2\right)^{1/2} + |\rho| v_1 \left(\pi - \arccos(|\rho| v_1)\right)\right]}{\left(1-|\rho|^2 v_1^2\right)^{3/2}} \qquad v_1 \in [-1, 1] \tag{4.7}$$

$$p_{v_2}(v_2) = \frac{1}{\pi\sqrt{1-v_2^2}} \frac{\left(1-|\rho|^2\right)\left[\left(1-|\rho|^2\left(1-v_2^2\right)\right)^{1/2} + |\rho|\sqrt{1-v_2^2}\left(\frac{\pi}{2} - \arccos(|\rho|\sqrt{1-v_2^2})\right)\right]}{\left(1-|\rho|^2\left(1-v_2^2\right)\right)^{3/2}} \qquad v_2 \in [-1, 1] \tag{4.8}$$

where $|\rho|$ denotes the coherence between the SAR images S_1 and S_2. A detailed derivation of these distributions is contained in Appendix A. In the following, a complete analysis of the noise terms v_1 and v_2 is presented.

4.2.1 Analysis of v_1

The term $\cos(v)$, denoted in the following as v_1, can be considered as the real part of the interferometric phasor noise within the complex plane. The pdf of this term depends only on the coherence value $|\rho|$, as it can be observed from Eq. (4.7). If the interferometric phase is analyzed within the real interval $[\phi_x - \pi, \phi_x + \pi)$, the coherence gives information about the noise content, in such a way that the smaller the coherence the larger the phase noise variance. Nevertheless, the effect of coherence over the pdf of v_1 is completely different. First of all, the limits of $p_{v_1}(v_1)$ as a function of the coherence are

$$\lim_{|\rho|\to 0} p_{v_1}(v_1) = \frac{1}{\pi\sqrt{1-v_1^2}} \qquad v_1 \in [-1,1] \tag{4.9}$$

$$\lim_{|\rho|\to 1} p_{v_1}(v_1) = \delta(v_1 - 1) \qquad v_1 \in [-1,1]. \tag{4.10}$$

Figure 4.1a depicts $p_{v_1}(v_1)$ for the complete range of coherences, where the limits given by Eqs. (4.9) and (4.10) can be clearly identified. Consequently, the coherence value varies the symmetry of the distribution of v_1 within the interval $[-1, 1]$.

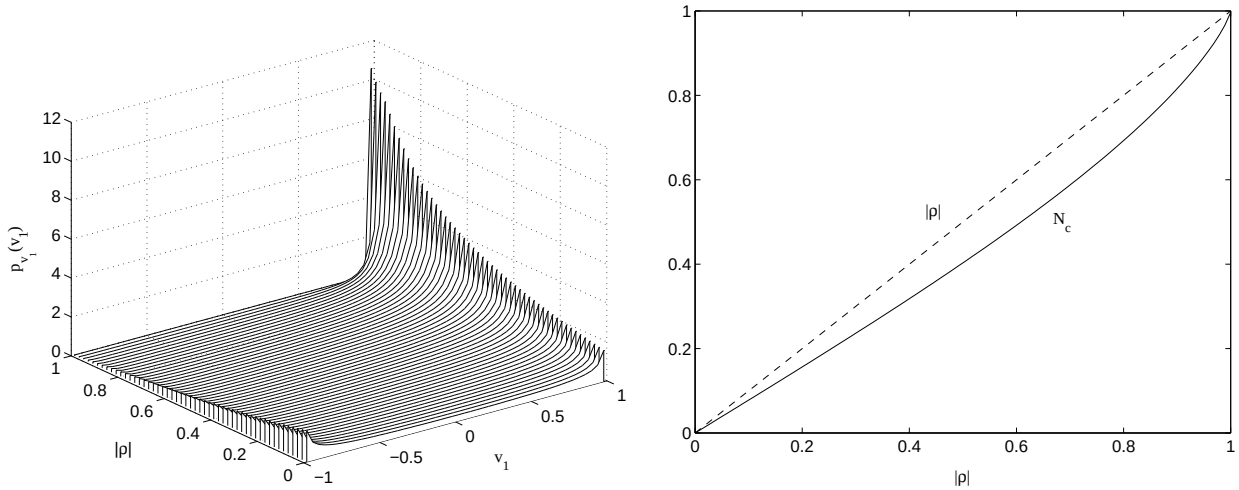

Figure 4.1: (a) Evolution of $p_{v_1}(v_1)$ as a function of the coherence value $|\rho|$. (b) Mean value of v_1, N_c.

The variation of the distribution's symmetry has a clear effect on the moments of v_1. Appendix B contains a detailed derivation of the mean value of v_1, whose value, for single-look SAR imagery, follows [170, 169]

$$N_c = E\{v_1\} = \frac{\pi}{4}|\rho|\ {}_2F_1\left(\frac{1}{2}, \frac{1}{2}; 2; |\rho|^2\right) \tag{4.11}$$

where ${}_2F_1(a, b; c; z)$ represents the Gauss hypergeometric function [171], see Appendix B for its definition. Figure 4.1b depicts the plot of the parameter N_c. From this figure, one can notice that despite the complex dependence of N_c on $|\rho|$, both parameters present similar values. A first consequence that can be extracted is that N_c may be employed as a new quality parameter, since it gives the same type of information that the coherence offers.

As it has been performed for the expression of the mean value of v_1, the variance, $\sigma^2_{v_1}$, can be obtained by deriving the second moment of v_1. Appendix B contains the detailed derivation of $\sigma^2_{v_1}$, where it can be seen the complexity of its expression, which includes an infinite series of hypergeometric functions. From a practical point of view, this expression gives no clear insights concerning the dependence of $\sigma^2_{v_1}$ on the coherence. Hence, it is worthwhile to find an approximation to the value of $\sigma^2_{v_1}$ with a simpler expression. Figure 4.2a gives the graphic of the actual value of $\sigma^2_{v_1}$. As it can concluded from this figure,

the exact variance value can easily be approximated by the following family of functions

$$\sigma^2_{v_1} \propto \frac{1}{2}(1-|\rho|^2)^{\alpha} \tag{4.12}$$

where α controls the shape of the function. By minimizing the square error between the actual value of $\sigma^2_{v_1}$ and the value given by Eq. (4.12) it is found that a minimum square error is attained for $\alpha = 0.79$. Figure 4.2 shows the true and the approximated values of $\sigma^2_{v_1}$, as well as the error between both curves for $\alpha = 0.79$. As it can be observed in Fig. 4.2, the approximation presents a small absolute error.

Any random variable with a non-zero mean value, can be expressed as the addition of this mean value plus a zero-mean random variable [72]. Consequently, v_1 can be written as follows

$$v_1 = N_c + v_1' \tag{4.13}$$

where v_1' denotes a zero-mean random variable with a variance equal to

$$\sigma^2_{v_1'} = \frac{1}{2}(1-|\rho|^2)^{0.79}. \tag{4.14}$$

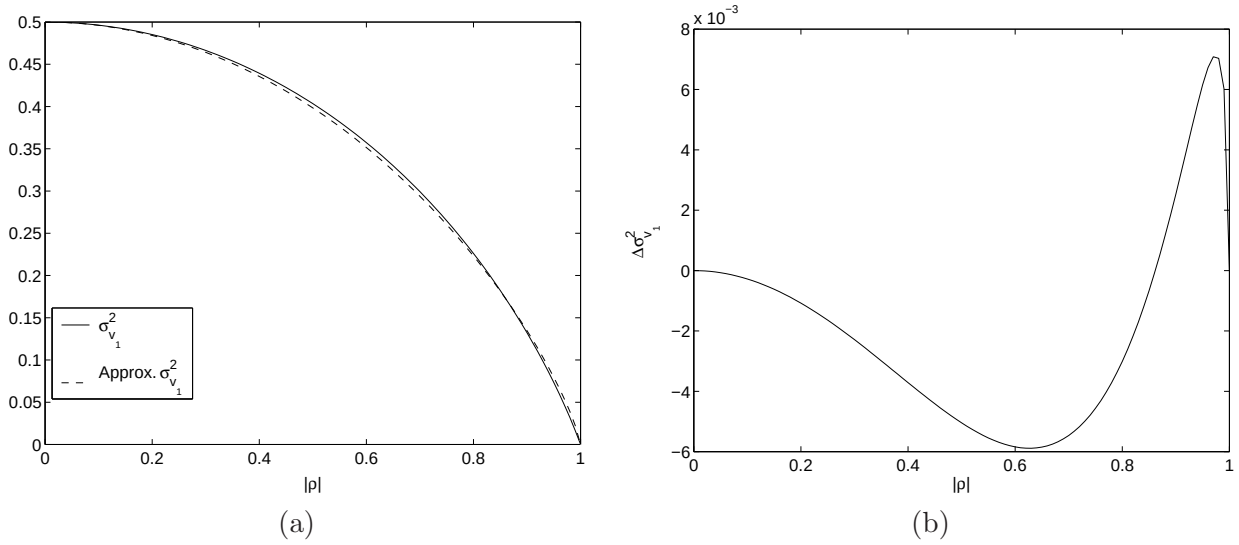

Figure 4.2: (a) Actual and approximated values for $\sigma^2_{v_1}$. (b) Approximation absolute error. In both cases $\alpha = 0.79$.

4.2.2 Analysis of v_2

Similarly, the term $\sin(v)$, denoted as v_2 in the following, can be considered as the imaginary part of the interferometric phase noise in the complex plane. As it can be observed from the pdfs given by Eqs. (4.7) and (4.8), the term v_2 has a different behavior compared with v_1. The limits of $p_{v_2}(v_2)$ with the coherence are

$$\lim_{|\rho|\to 0} p_{v_2}(v_2) = \frac{1}{\pi\sqrt{1-v_2^2}} \qquad v_2 \in [-1,1] \tag{4.15}$$

$$\lim_{|\rho|\to 1} p_{v_2}(v_2) = \delta(v_2) \qquad v_2 \in [-1,1]. \tag{4.16}$$

Fig. 4.3 represents $p_{v_2}(v_2)$ for the complete range of coherences. It can be observed, that for low coherences $p_{v_1}(v_1)$ and $p_{v_2}(v_2)$ present a very similar behavior due to the uniform distribution of the interferometric phase difference. On the contrary, as the coherence increases, $p_{v_1}(v_1)$ is concentrated around $v_1 = 1$, whereas $p_{v_2}(v_2)$ is concentrated around $v_2 = 0$, since the interferometric phase noise

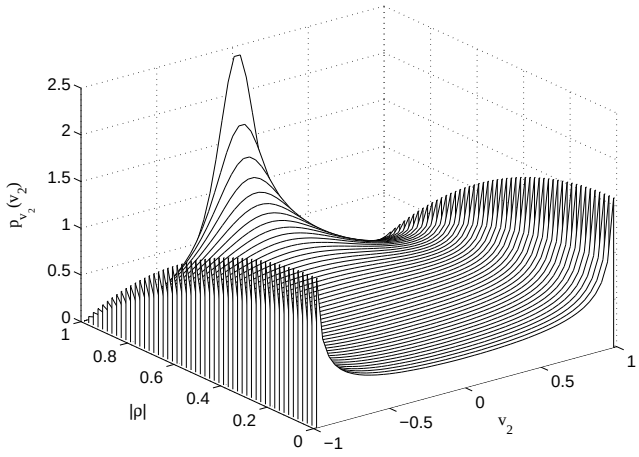

Figure 4.3: Evolution of $p_{v_2}(v_2)$ as a function of coherence value $|\rho|$.

becomes a delta function around $v = 0$ rad. Hence, the moments of v_2 will present a different dependence comparing them with the moments of v_1.

The distribution $p_{v_2}(v_2)$, as given by Fig. 4.3, is symmetric for any coherence value. Consequently, its mean value, denoted by N_s, is always equal to zero. On the other hand, the variance value, called $\sigma^2_{v_2}$, can be easily derived from $\sigma^2_{v_1}$ by considering the equality $E\{\cos^2(v)\} = \sigma^2_{v_1} + N_c^2$

$$\sigma^2_{v_2} = E\{\sin^2(v)\} = E\{1 - \cos^2(v)\} = \left(1 - N_c^2\right) - \sigma^2_{v_1}. \tag{4.17}$$

Once again, the expression of $\sigma^2_{v_2}$ presents a complicate dependence with respect to the coherence, by considering the expressions of N_c and $\sigma^2_{v_1}$, which makes a difficult task to extract any type of conclusion. Fig. 4.4a presents the graphic of $\sigma^2_{v_2}$ as a function of the coherence $|\rho|$. Also in this case, an approximate curve for the actual value of $\sigma^2_{v_2}$ has been found. Owing to the dependence of $\sigma^2_{v_2}$ on the coherence, the same family of functions employed to approximate $\sigma^2_{v_1}$, see Eq. (4.12), has been selected. Also, a minimum square error criteria has been adopted to find the value of α which best approximates $\sigma^2_{v_2}$. In this case, the minimum is attained for $\alpha = 0.58$. Fig. 4.4 presents the graphic of this approximation, as well as the absolute error between the actual and the approximate values of $\sigma^2_{v_2}$. As it can be seen from Fig. 4.4b, this error presents very small values.

Therefore, the random process v_2, which will be denoted by v_2' in the following to maintain the parallelism with v_1, can be analyzed as a zero-mean random process with a variance given by

$$\sigma^2_{v_2'} = \frac{1}{2}(1 - |\rho|^2)^{0.58}. \tag{4.18}$$

It is worth to remark that within Section 4.2.1 it has been proved that v_1 can be decomposed as $v_1 = N_c + v_1'$. Consequently, v_1' can be considered as a noise source which corrupts the useful information content, given by N_c. Section 4.2.2 showed that, since v_2 has a mean value equal to zero, it can be only considered as a noise source. These decompositions are now introduced within Eqs. (4.5) and (4.6) as follows

$$\cos(\phi) = N_c \cos(\phi_x) + v_1' \cos(\phi_x) - v_2' \sin(\phi_x) \tag{4.19}$$
$$\sin(\phi) = N_c \sin(\phi_x) + v_1' \sin(\phi_x) + v_2' \cos(\phi_x). \tag{4.20}$$

The parameter N_c, as well as the processes v_1' and v_2' have been exclusively derived from the interferometric phase noise v. Therefore, in principle, they are considered as noise components which corrupts the useful signal given by $\cos(\phi_x)$ and $\sin(\phi_x)$. Since v_1' and v_2' are zero-mean random variables, one can prove that

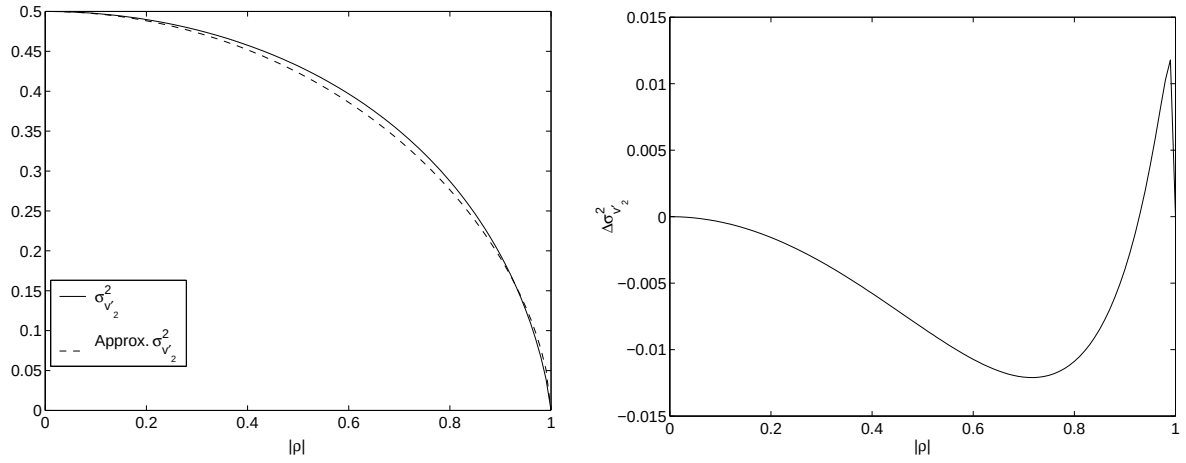

Figure 4.4: (a) Exact and approximated values for $\sigma^2_{v_2}$. (b) Approximation absolute error. In both cases $\alpha = 0.58$.

despite the second and third addends of Eqs. (4.19) and (4.20) contain useful information [1], this is lost. Assuming an homogeneous interferometric phase, as well as homogeneous noise

$$E\{v_1' \cos(\phi_x) - v_2' \sin(\phi_x)\} = E\{v_1'\}\cos(\phi_x) - E\{v_2'\}\sin(\phi_x) = 0 \quad (4.21)$$

$$E\{v_1' \sin(\phi_x) + v_2' \cos(\phi_x)\} = E\{v_1'\}\sin(\phi_x) + E\{v_2'\}\cos(\phi_x) = 0. \quad (4.22)$$

Therefore, as these terms do not contain information at all, two new noise terms can be defined as follows

$$v_c = v_1' \cos(\phi_x) - v_2' \sin(\phi_x) \quad (4.23)$$

$$v_s = v_1' \sin(\phi_x) + v_2' \cos(\phi_x). \quad (4.24)$$

These two noise terms have, as it will be presented in the following, a more similar behavior between them than v_1 and v_2 have.

With the introduction of the noise terms v_c and v_s, the real and imaginary parts of the interferometric phasor, Eqs. (4.5) and (4.6), can be written as [170, 169]

$$\Re\{e^{j\phi}\} = N_c \cos(\phi_x) + v_c \quad (4.25)$$

$$\Im\{e^{j\phi}\} = N_c \sin(\phi_x) + v_s. \quad (4.26)$$

These two equations represent the noise model for the real and imaginary parts of the measured interferometric phasor. The useful information, given by $\cos(\phi_x)$ and $\sin(\phi_x)$ is first affected by the term N_c in a multiplicative way. Additionally, this product is also contaminated by the additive noise terms v_c and v_s. Consequently, this new interferometric phasor noise model is characterized for being a linear noise model.

The noise terms v_c and v_s have a double dependence. On the one hand, the variance of these terms depend on the interferometric phase ϕ_x, as it can be deduced from Eqs. (4.23) and (4.24). On the other hand, the variance depends also on the coherence $|\rho|$, as the terms v_1' and v_2' depend on it. By considering v_c and v_s as zero-mean value terms, it follows that their variances can be obtained as

$$\sigma^2_{v_c} = E\left\{\left(v_1' \cos(\phi_x) - v_2' \sin(\phi_x)\right)^2\right\} = \sigma^2_{v_1'} \cos^2(\phi_x) + \sigma^2_{v_2'} \sin^2(\phi_x) \quad (4.27)$$

$$\sigma^2_{v_s} = E\left\{\left(v_1' \sin(\phi_x) + v_2' \cos(\phi_x)\right)^2\right\} = \sigma^2_{v_1'} \sin^2(\phi_x) + \sigma^2_{v_2'} \cos^2(\phi_x) \quad (4.28)$$

[1] Given by the parameters $\cos(\phi_x)$ and $\sin(\phi_x)$

where the equality $E\{v_1' v_2'\} = E\{(v_1 - N_c)v_2\} = 0$ has been included. The values of $\sigma^2_{v_c}$ and $\sigma^2_{v_s}$ will vary, for any coherence value, between the values of $\sigma^2_{v_1'}$ and $\sigma^2_{v_2'}$ according to the value of ϕ_x. Hence, since $\sigma^2_{v_1'}$ and $\sigma^2_{v_2'}$ present similar values, the dependence of v_c and v_s on ϕ_x can be cancelled out by properly approximating the value of their respective variances. As proved in Appendix C, $\sigma^2_{v_c}$ and $\sigma^2_{v_s}$ can be approximated by the family of curves given by Eq. (4.12). In this case, the exponent α is the average value of the exponents of the curves of $\sigma^2_{v_1'}$ and $\sigma^2_{v_2'}$. Hence

$$\sigma^2_{v_c} = \sigma^2_{v_s} = \frac{1}{2}(1 - |\rho|^2)^{0.685} \tag{4.29}$$

Selecting this curve, first, the average error with respect to the actual values of $\sigma^2_{v_c}$ and $\sigma^2_{v_s}$ is minimized, and second, the additive noise terms in the real and imaginary parts will present the same behavior [169]. Fig. 4.5 presents the curves of $\sigma^2_{v_1'}$ and $\sigma^2_{v_2'}$ as well as the approximation for $\sigma^2_{v_c}$ and $\sigma^2_{v_s}$.

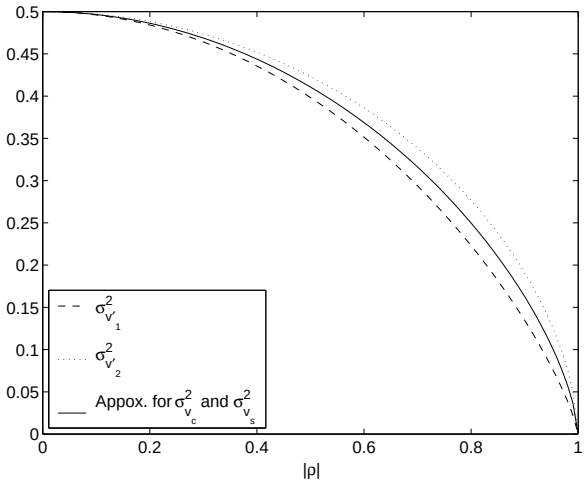

Figure 4.5: Curves of $\sigma^2_{v_1'}$ and $\sigma^2_{v_2'}$ and the approximated values of $\sigma^2_{v_c}$ and $\sigma^2_{v_s}$.

The interferometric phasor noise model, represented by Eqs. (4.25) and (4.26), can be also expressed as a sum of complex phasors

$$e^{j\phi} = N_c e^{j\phi_x} + (v_c + jv_s). \tag{4.30}$$

Fig. 4.6 displays a representation of Eq. (4.30). The amplitude of the true interferometric phasor is multiplied by the parameter N_c. Therefore, this parameter affects the amplitude but not the phase of the true interferometric phasor. On the contrary, the additive noise phasor $v_c + jv_s$ affects both, the amplitude and the phase of the true interferometric phasor. Since the term $N_c e^{j\phi_x}$ contains information concerning coherence and phase, it will be called in the following as *Modulated Coherence Term*.

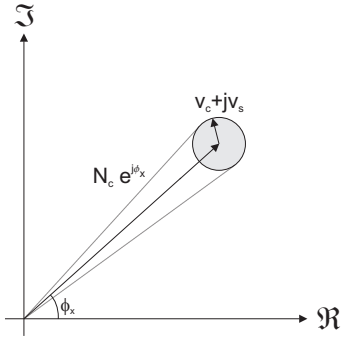

Figure 4.6: Representation of the interferometric phasor noise model.

4.2.3 Interferometric Phasor Noise Model Validation

A new noise model for the interferometric phasor, whose expression is given by Eq. (4.30), has been proposed in the previous section. In the following, a validation of this model is performed by using both, simulated as well as real InSAR data. On the one hand, simulated data are employed as it offers the possibility to reproduce any signal condition and access to the original signal, which is pretended to be recovered, is feasible. On the other hand, the noise model is also tested with real InSAR data.

Interferometric Phasor Noise Model Validation: Simulated InSAR Data

An homogeneous SAR image, under the assumption of fully developed speckle for distributed scatterers, can be modelled by $\mathcal{N}_c(0, \sigma^2/2)$. On the other hand, InSAR data are generated from the combination of correlated SAR images acquired from slightly different positions, in such a way that the degree of correlation determines the phase difference noise power. Consequently, InSAR data can be simulated as follows [172, 37]:

- First, the complex, two-dimensional array of independent, zero-mean, Gaussian distributed variables
$$\mathbf{k}' = [\ S_1 \quad S_2\ ]^T \tag{4.31}$$
is generated, where $S_1 = S_{11} + jS_{12}$ and $S_2 = S_{21} + jS_{22}$. The components S_{11}, S_{12}, S_{21} and S_{22} denote independent, zero-mean Gaussian distributed variables, $\mathcal{N}(0, \sigma^2)$.
- The second step consists in the generation of correlated, zero-mean, complex Gaussian variables from the set of uncorrelated variables. The generation of these correlated variables is based on the method presented in [172], where the vector of correlated components is obtained as
$$\mathbf{k} = \sigma_{S_1} \begin{bmatrix} 1 & 0 \\ \rho^* \sqrt{\gamma} & \sqrt{\gamma(1-|\rho|^2)} \end{bmatrix} \begin{bmatrix} S_1 \\ S_2 \end{bmatrix} \tag{4.32}$$
where
$$\sigma_{S_1} = E\{|S_1|^2\} \quad \gamma = \frac{E\{|S_2|^2\}}{E\{|S_1|^2\}} \quad \rho = \frac{E\{S_1 S_2^*\}}{\sqrt{E\{|S_1|^2\}E\{|S_2|^2\}}} \tag{4.33}$$
The parameters σ_{S_1} and γ refer to the power of each one of the SAR images. These parameters can be set to 1 as interest is focused on the phase of the product $S_1 S_2^*$. The coefficient ρ refers to the complex correlation coefficient between both SAR images. Therefore, it is possible to simulate InSAR data for any correlation coefficient setting its amplitude to any value between 0 and 1, and setting an arbitrary value for the interferometric phase ϕ_x. As homogeneous data will be simulated, ρ is constant for the complete image. Nevertheless, non homogeneous InSAR data can be also simulated.
- The simulated interferometric phase is taken as the phase of the complex conjugated product $S_1 S_2^*$, whose value, free of noise effects, is ϕ_x.

The previous algorithm has been employed to simulate InSAR data for different values of the complex correlation coefficient. In all the cases, simulated data correspond to 512 by 512 pixel SAR images.

The process to test the validity of the proposed noise model, given by Eqs. (4.25) and (4.26), consists in comparing real statistics obtained from simulated data with those proposed by the noise model in the basis of a Monte-Carlo method. On the one hand, real statistics are obtained over 7 by 7 pixel non-overlapped windows. The size of these windows provide sufficient statistics to calculate the mean and the variance of data [113]. The mean value corresponds to the products $N_c \cos(\phi_x)$ and $N_c \sin(\phi_x)$ for the real and imaginary parts of the interferometric phasor respectively. The variance of the additive noise terms v_c and v_s, is approximated by Eq. (4.29). The validity test allows to analyze also the effects of this approximation.

The first test consists in the simulation of an interferometric phase of value $\phi_x = \pi/4$. The interest of this value lies in the fact that no error is introduced on $\sigma^2_{v_c}$ and $\sigma^2_{v_s}$, since $\cos^2(\phi_x) = \sin^2(\phi_x) = 1/2$. The results corresponding to this test are presented in Fig. 4.7. Respect to the mean values, a complete agreement between the theoretical data, given by the solid line, and the values obtained from the simulated data is observed. Error bars represent the standard deviation of the mean value estimator, which corresponds to the sample mean in the 7 by 7 pixel windows [72,173]. No differences are observed between the real and imaginary parts. The variance of the additive noise terms v_c and v_s has been estimated by the classical sample variance estimator in 7 by 7 pixel windows [72, 173]. As it can be observed from Figs. 4.7c and 4.7d, the values given by the approximation introduced by Eq. (4.29), are very close to the actual values.

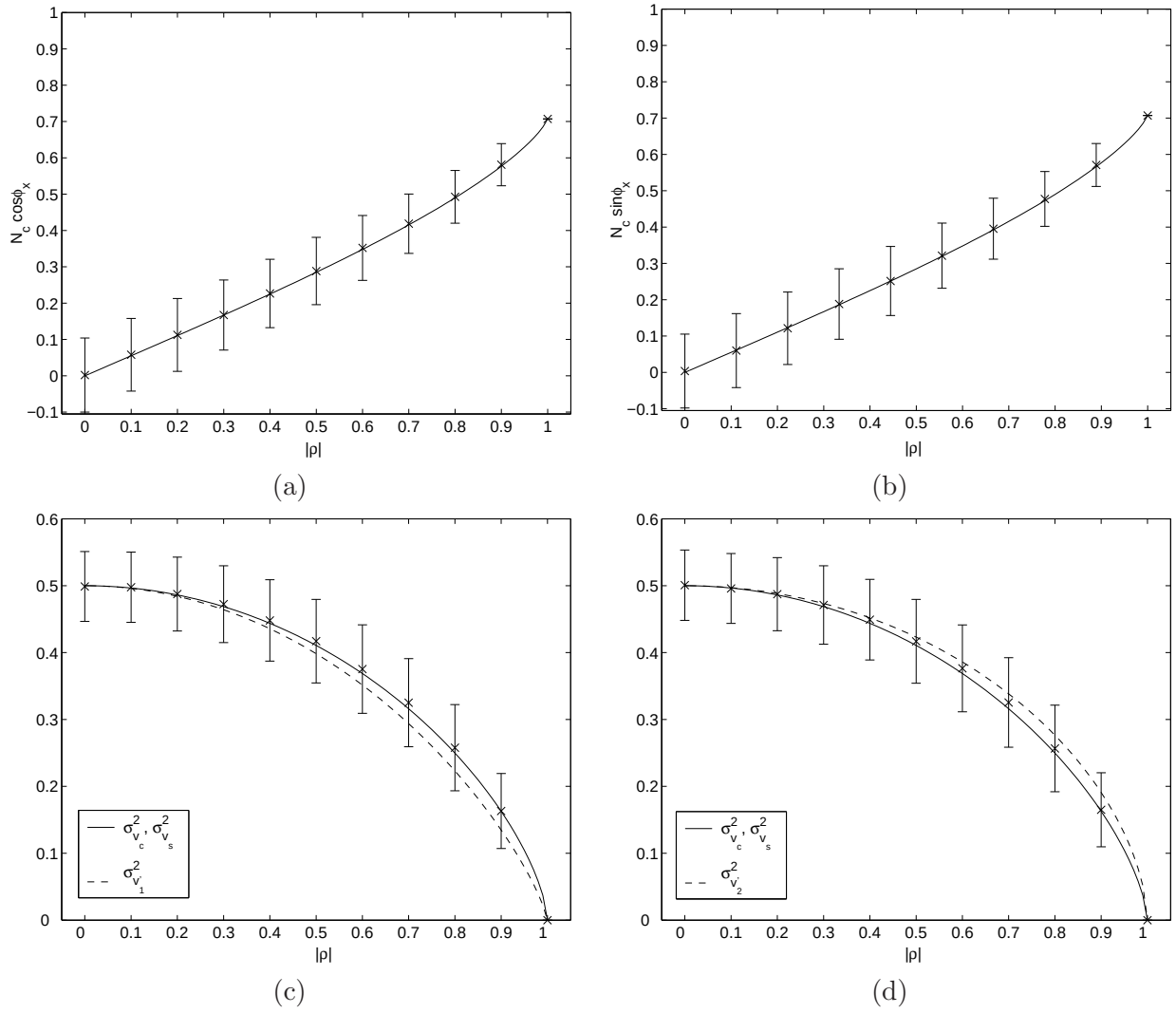

Figure 4.7: Monte-Carlo analysis to test the validity of the interferometric phasor noise model. Solid lines represent actual values, whereas dashed lines represent the approximated values for the variances $\sigma^2_{v'_1}$ and $\sigma^2_{v'_2}$. Error bars represent the variances of the calculated statistics. (a) Real part mean value ($N_c \cos(\phi_x)$). (b) Imaginary part mean value ($N_c \sin(\phi_x)$). (c) Real part variance. (d) Imaginary part variance. It is important to notice that the mean values (a) and (b) present a maximum value close to 0.7 as a consequence of the homogeneous interferometric phase.

The agreement between the statistics of the simulated interferometric phase, calculated with the sample estimators, and the statistics given by the proposed noise model have been also quantitatively measured by a first order least squares regression analysis. The interpretation of each one of the coefficients of this analysis can be found in Appendix D. In this case, for each one of the 7 by 7 pixel windows, the coherence value is calculated, from which the theoretical values of the mean and the variance, re-

		a_0	a_1	s	r
$\Re\{e^{j\phi_x}\}$	Mean	-0.001	1.003	0.056	0.976
	Variance ($\sigma^2_{v_c}$)	0	1.003	0.056	0.970
$\Im\{e^{j\phi_x}\}$	Mean	-0.040	1.048	0.058	0.935
	Variance ($\sigma^2_{v_s}$)	-0.039	1.046	0.058	0.935

Table 4.1: Least squares regression analysis of the statistics corresponding to the simulated interferometric phase $\phi_x = \pi/4$.

		a_0	a_1	s	r
$\Re\{e^{j\phi_x}\}$	Mean	0.002	1.002	0.056	0.984
	Variance ($\sigma^2_{v_c}$)	0	1.005	0.056	0.762
$\Im\{e^{j\phi_x}\}$	Mean	-0.057	1.062	0.070	0.913
	Variance ($\sigma^2_{v_s}$)	-0.021	1.032	0.045	0.959

Table 4.2: Least squares regression analysis of the statistics corresponding to the simulated interferometric phase $\phi_x = 0$.

spectively given by Eqs. (4.11) and (4.29), are obtained. Table 4.1 shows the full agreement between the real statistics and the theoretical values derived from the estimated coherence value. The values corresponding to the least squares regression lines, a_0 and a_1, correspond to a complete mach between actual and estimated values, for the mean as well as for the variances. Moreover, the deviation around these regression lines presents low values. Finally, the coefficient of correlation r, which gives an overall measurement of the correlation between real and theoretical values, presents very high values in all the cases. Of especial interest is the coefficient of correlation corresponding to the regression analysis of the variance values. Despite the approximation introduced in the value of the variance, a total agreement with the actual values is obtained.

The accuracy and the effects of the approximation introduced for the values of the variances $\sigma^2_{v_c}$ and $\sigma^2_{v_s}$ is now examined by two additional analysis. First of all, an interferometric phase of value $\phi_x = 0$ has been simulated for the complete range of coherences in a similar way as it has been shown above. The interest on simulating the value of this phase lies in the fact that the actual values of $\sigma^2_{v_c}$ and $\sigma^2_{v_s}$ present the maximum deviation with respect to the approximated values given by Eq. (4.29). Therefore, a regression analysis is employed to compare the exact statistics obtained from the data and the corresponding approximate values. Table 4.2 presents the results of this regression analysis. As it can be observed, the correlation between the approximated values of $\sigma^2_{v_c}$ and $\sigma^2_{v_s}$ and their actual values are high, as it can be deduced from the coefficient of correlation r.

A second analysis has consisted of simulating a 1024 by 1024 pixel homogeneous interferometric phase with a coherence $|\rho| = 0.7$. In this case, the interferometric phase corresponds to a constant slope producing a 400 pixel phase fringes. In this situation, the coherence calculation does not present underestimation problems [113] and the interferometric phase ϕ_x contains all the possible values in the range $[-\pi, \pi)$. The actual mean and variance values are estimated by the usual sample estimators in a 7 by 7 pixel window. Fig. 4.8 presents the standard deviation values as a function of the mean value, for the real part of the interferometric phasor. Also, the theoretical relations for the cases in which $\cos(\phi_x)$ is equal to 0, ± 1, $\pm .5$ and $\pm\sqrt{3}/2$ are included. According to Fig. 4.8, it can be observed that the actual value of σ_{v_c} is almost independent of the phase value $\cos(\phi_x)$. The curvature at the extremes of the cloud of points is due to the dependence between N_c and σ_{v_c}, since both terms depend on the coherence value [169]. This fact helps to confirm the approximation of $\sigma^2_{v_c}$ and $\sigma^2_{v_s}$ as the mean value of the variances $\sigma^2_{v'_1}$ and $\sigma^2_{v'_2}$, Eq. (4.29), due to its similar values.

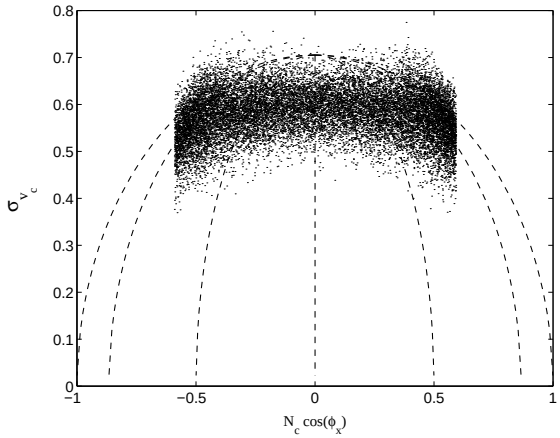

Figure 4.8: Representation of the term σ_{v_c} as a function of the mean value $N_c \cos(\phi_x)$ for a 1024 by 1024 interferometric phase with an slope producing 400-pixel fringes, with a coherence equal to 0.7.

Interferometric Phase Noise Model Validation: Real InSAR Data

In addition to the validation process presented within the previous section, the proposed noise model for the interferometric phasor has been also tested over real InSAR data [170, 169]. The data employed in this section correspond to a 1024 by 1024 pixel, X-band, single pass interferogram of Mt. Etna (Italy) with an approximate baseline of 80 cm, see Fig. 4.9. These data were acquired by the E-SAR system, operated by the German Aerospace Center (DLR).

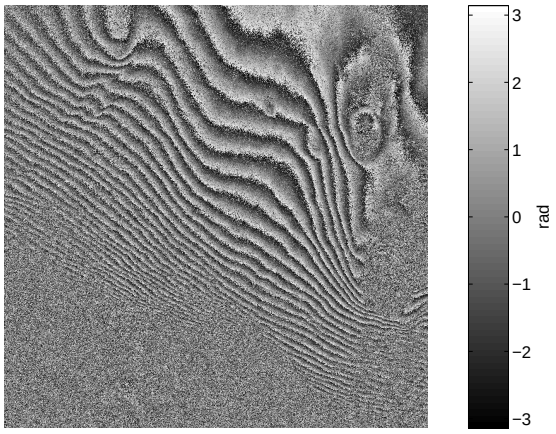

Figure 4.9: Mt. Etna X-band interferometric phase.

As it has been performed in the simulated data case, the interferometric phasor noise model is tested by comparing the mean and standard deviation obtained from data, with the theoretical values derived from the corresponding coherence value. The mean values, as it can be seen from Eqs. (4.25) and (4.26) depend on the phase value ϕ_x. Hence, for the purpose of simplifying the analysis, only those cases in which $\cos(\phi_x)$ is equal to 0, 0.5 and 0.9 for the real part model and $\sin(\phi_x)$ is equal to 0, 0.5 and 0.9 for the imaginary part model have been considered. The calculated statistics, as well as the theoretical values given by the proposed model are presented in Fig. 4.10 for the real and imaginary parts of the interferometric phasor. As it can be seen, the actual values completely fit the theoretical relation between the mean and the standard deviation, confirming the validity and accuracy of the proposed model to describe the behavior of the interferometric phasor.

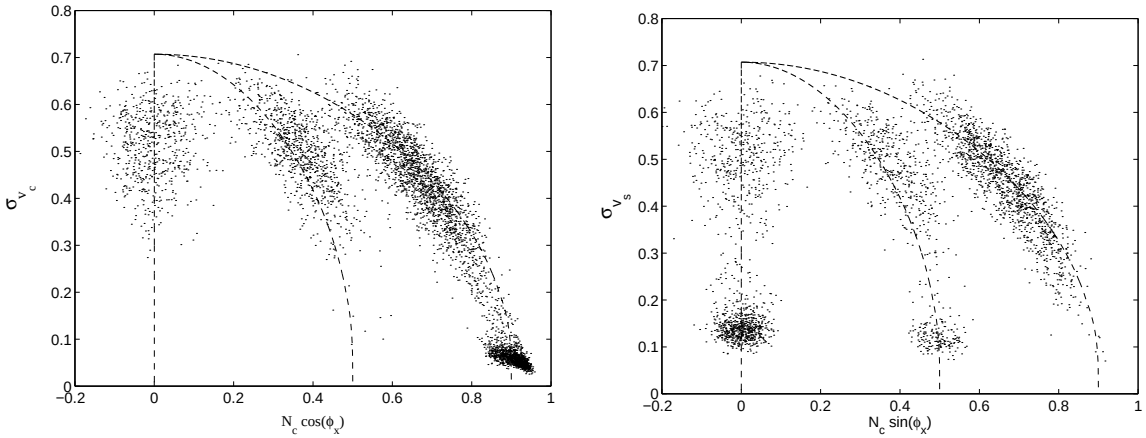

(a) (b)

Figure 4.10: Interferometric phasor noise model validation over Mt. Etna data. Dashed lines represent the theoretical relation between the mean and the variance values of the interferometric phasor components. The clouds of points represent the real values calculated by the 7 by 7 pixel sample estimators. (a) Real part interferometric phasor components. (b) Imaginary part interferometric phasor components.

4.2.4 Multilook Interferometric Phasor Noise Model

The measured interferometric phasor noise model given by Eq. (4.30) concerns noise description for single-look data. Sometimes, on the contrary, SAR data are not available with this format but as multilook data, which is obtained at the expense of spatial resolution. Hence, the ideas introduced throughout this section with the objective to describe the noise processes for single-look data, are extended for the description of the multilook interferometric phasor.

The pdf corresponding to the multilook interferometric phase can be derived from the complex Wishart distribution $\mathcal{W}([C], N)$, see Eq. (2.181) at page 46. This distribution describes the statistical behavior of correlated SAR images. Considering a non-diagonal element $S_1 S_2^*$ of the covariance matrix and integrating over the amplitude, the expression of the multilook interferometric phase is

$$p_\phi(\phi) = \frac{\Gamma(N+1/2)(1-|\rho|^2)^N \beta}{2\sqrt{\pi}\Gamma(N)(1-\beta^2)^{N+1/2}} + \frac{(1-|\rho|^2)^N}{2\pi} {}_2F_1(N, 1; 1/2; \beta^2) \;\; \phi \in [-\pi, \pi) \tag{4.34}$$

where $\beta = |\rho|\cos(\phi - \phi_x)$ and N represents the number of looks. As for the single-look case, the previous distribution has its mode at ϕ_x. It is important to notice, that the dependence of Eq. (4.34) on the phase ϕ and on the mode ϕ_x is independent of the number of looks. Consequently, for the multilook case, the measured interferometric phase can be still be expressed as the addition of an information bearing component, ϕ_x, plus an independent noise term v, see Eq. (4.1) [94]. The effect of the number of looks is to change the behavior of the noise term v in such a way that the larger the number of looks the lower the noise variance around the phase mode ϕ_x, for the phase considered at the interval $[\phi_x - \pi, \phi_x + \pi)$. The main consequence of the maintenance of the additivity of the noise model for the interferometric phase ϕ_x is, that, the introduced interferometric phasor noise model for single-look data, Eq. (4.30), is equally valid for multilook data. However, the value of N_c, as well as the statistical properties of the additive noise terms v_c and v_s need additional revision.

Appendix B presents the derivation of the parameter N_c for an arbitrary number of looks. Fig. 4.11 shows the evolution of N_c respect to the coherence and with respect to the number of looks. As it can be observed, the parameter N_c is a quality measure of the phase, as it depends both on the coherence and on the number of looks. For values close to one it indicates that phase is not affected by noise. This is accomplished for data presenting a large coherence value or by increasing the number of averaged pixels. In any case, given the number of looks, it is possible to recover the exact value of the coherence by inverting the expression of N_c.

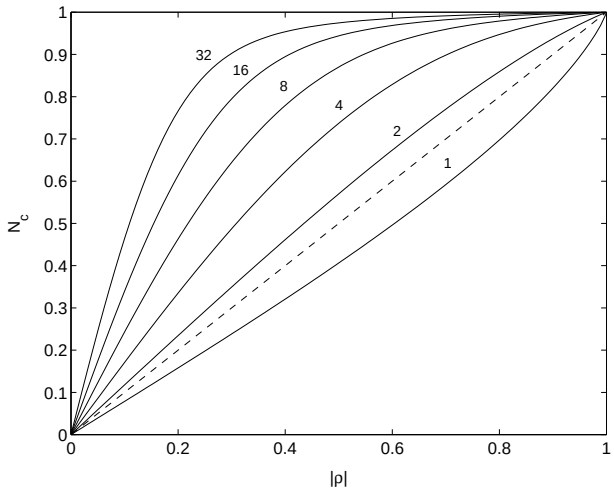

Figure 4.11: Evolution of the parameter N_c as a function of the coherence $|\rho|$ and the number of looks N. The dashed line represents the coherence, whereas solid lines represent N_c for a given number of looks, indicated by the number at each curve.

The number of looks also affects the behavior of the noise terms v'_1 and v'_2, see Sections 4.2.1 and 4.2.2. By construction, these two terms present a mean equal to zero for any number of looks. As it has been made evident for the single-look case, $\sigma^2_{v'_1}$ and $\sigma^2_{v'_2}$ present complex expressions difficult to handle. The introduction of the number of looks within the interferometric phase difference pdf, Eq. (4.34), makes the Gauss hypergeometric function to appear, which complicates even more the final expressions for $\sigma^2_{v'_1}$ and $\sigma^2_{v'_2}$. For this reason, numerical integration techniques have been employed to obtain the values of $\sigma^2_{v'_1}$ and $\sigma^2_{v'_2}$ as a function of the number of looks and the coherence, see Fig. 4.12. As presented by Eqs.

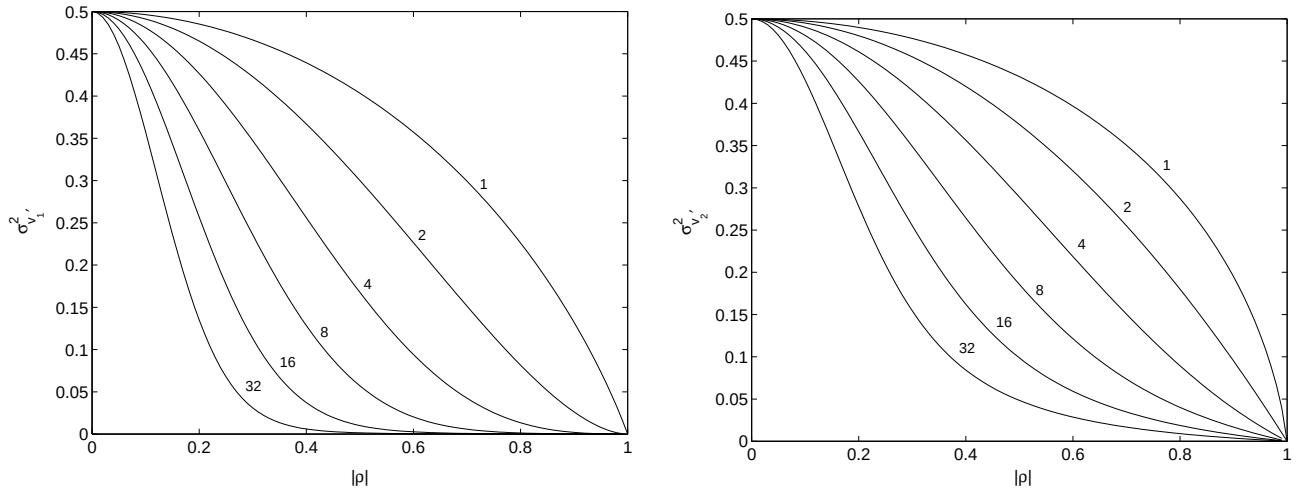

Figure 4.12: Variances of terms v'_1 and v'_2 as a function on the number of looks (indicated by the numbers) and the coherence. (a) Real part noise variance $\sigma^2_{v'_1}$. (b) Imaginary part noise variance $\sigma^2_{v'_2}$.

(4.23) and (4.24), the noise terms v'_1 and v'_2 are combined to form two new noise terms denoted by v_c and v_s. The way v'_1 and v'_2 are combined depends on the interferometric phase value ϕ_x. Nevertheless, the closeness of the values $\sigma^2_{v'_1}$ and $\sigma^2_{v'_2}$ for the whole coherence range, has made possible, for single-look data, to get rid of this dependence by assuming v_c and v_s to have the same variance value and equal to the mean value of $\sigma^2_{v'_1}$ and $\sigma^2_{v'_2}$. In the case of multilook data this construction is still possible. Therefore, the interferometric phasor noise model, derived in this section and given by Eq. (4.30), is equally valid for multilook interferometric data.

The only point to consider with this generalization is the fact that the larger the number of looks, the larger the difference between the values of $\sigma^2_{v'_1}$ and $\sigma^2_{v'_2}$, as it can be seen in Fig. 4.12. This fact makes the approximated values of $\sigma^2_{v_c}$ and $\sigma^2_{v_s}$ to present a larger error with respect to the actual values. The reason behind this behavior is the dependence of the noise terms v_c and v_s on the value of the interferometric phase, see Eqs. (4.27) and (4.28). Therefore, the larger the number of looks, the larger the difference between the behavior of the noise terms v_c and v_s, making necessary to take into consideration this difference in the case a noise reduction technique is applied.

As a final conclusion, it can be observed from Figs. 4.11 and 4.12 that, even for a large number of looks, the noise content at low-coherence areas is still high. This indicates that to extract information from low-coherence areas is difficult. A way to extract this information could be to increase the number of looks, whose main consequence would be an important loss of spatial resolution. Hence, in these situations it is necessary to consider more advanced techniques in order to extract useful information with a minimum loss of spatial resolution.

4.3 Wavelet Interferometric Phasor Noise Model

The aim of the previous section has been to introduce, and to validate, a new linear noise model for the measured interferometric phasor. The availability of this noise model has made possible to identify noise sources and to determine how they degrade the useful signal component. Consequently, this section is focused on examining which is the best use of the interferometric phasor noise model from the point of view of information extraction.

As it has been presented throughout Chapter 3, the wavelet analysis theory, and specially the discrete wavelet transform (DWT), are powerful tools to analyze non homogeneous functions in a space-frequency frame. The development which will be presented in this section shows the suitability of the wavelet theory for the interferometric phasor noise problem. Previous to this analysis, it is valuable to present a brief summary underlying the main reasons which justify the use of the wavelet theory in this case [169]:

- The wavelet transform is employed as it will offer the possibility to use the parameter N_c as an important source of interferometric information. Indeed, this parameter will be shown to be valid for the derivation of coherence information.
- The main advantage of SAR systems, compared with other remote sensing techniques, is the capability to obtain information from the Earth's surface, whatever the weather conditions and the day/night cycle, with a high spatial resolution. The main drawback, on the contrary, is the presence of speckle noise which makes the obtention of useful information a not evident task. Owing to these reasons, any process designed to reduce speckle noise has to maintain the spatial properties and the details of the data, that is, it has to maintain the spatial resolution. The wavelet transform is employed, therefore, to estimate the interferometric information with high spatial resolution.

This section concerns, therefore, the study of the interferometric phasor in the wavelet domain. First of all, a one-dimensional model for the true interferometric phasor is derived, from which a one-dimensional noise model for the interferometric phasor in the wavelet domain is presented. Subsequently, an extension to the two-dimensional case is derived and analyzed.

4.3.1 True Interferometric Phasor Model

For natural scenes, the interferometric phase is a non-homogenous and complex signal containing information related with topography, but also spatial details as for instance man-made structures. This complexity makes unattainable to derive a simple noise model for the interferometric phasor at the wavelet domain. In order to obtain this model, a simplification of the interferometric phase, which makes possible to perform a concise analysis about the interferometric phasor at the wavelet domain is introduced [170].

An interferogram is created as the complex conjugate product $S_1 S_2^*$, see Eq. (2.79) at page 26, where S_1 and S_2 represent each one of the complex SAR images. At Section 2.2.4, it was shown that both SAR images represent two frequency shifted versions of the terrain spectra. This shift, denoted by $\Delta\omega$ and called Wavenumber Shift [86], is proportional to the imaging geometry and to the local terrain's topography. Therefore, the interferogram's Fourier transform corresponds, ideally, to a delta function at the frequency $\Delta\omega$. At the space domain, the interferogram corresponds to a phasor at the frequency $\Delta\omega$. Hence, the interferometric phase difference ϕ_x, at the real plane, consists in a constant slope signal, whose slope is proportional to $\Delta\omega$. In fact, the measured interferometric phase does not correspond to a constant slope signal, but to a wrapped version within the interval $[-\pi, \pi)$ as a consequence of the periodic nature of the measured interferometric phase.

For the sake of simplicity, the one-dimensional interferometric phase difference signals are considered. In such a case, the non-wrapped interferometric phase can be modelled as a constant slope signal

$$\zeta_x[m] = \frac{2\pi}{N} m \tag{4.35}$$

where m is the spatial coordinate and $2\pi/N$ denotes the slope [2], which represents the Wavenumber Shift $\Delta\omega$. The real interferometric phase difference ϕ_x is measured in a wrapped form, hence

$$\phi_x[m] = \text{mod}\{\zeta_x[m] + \pi, 2\pi\} - \pi \tag{4.36}$$

where $\text{mod}\{\cdot, 2\pi\}$ refers to the modulus operation, in this case 2π-modulus. The signal $\phi_x[m]$ in Eq. (4.36) is ideally represented by a sawtooth signal, whose values range from $-\pi$ to π, with a N-pixel period. Fig. 4.13a depicts a one-dimensional interferometric phase with a 25-pixel period. Fig. 4.13b presents the Fourier transform amplitude of this interferometric phase, whereas Fig. 4.13c shows the Fourier transform amplitude of $\cos(\phi_x)$. The wrapped nature of the interferometric phase makes the useful signal to occupy the whole spectra. On the contrary, the signal $\cos(\phi_x)$ occupies only a small portion of it. From a point of view of noise reduction, by assuming white noise, the signal ϕ_x and the noise share all the spectra, making difficult to reduce noise without altering the useful signal. On the contrary, it is easier to reduce noise in the case of $\cos(\phi_x)$, which corresponds to the first harmonic of the wrapped phase ϕ_x, since this signal shares only a small portion of the spectra with the noise. It can be concluded, in the light of this result, that it is worthwhile to define a noise model for the interferometric phasor [170].

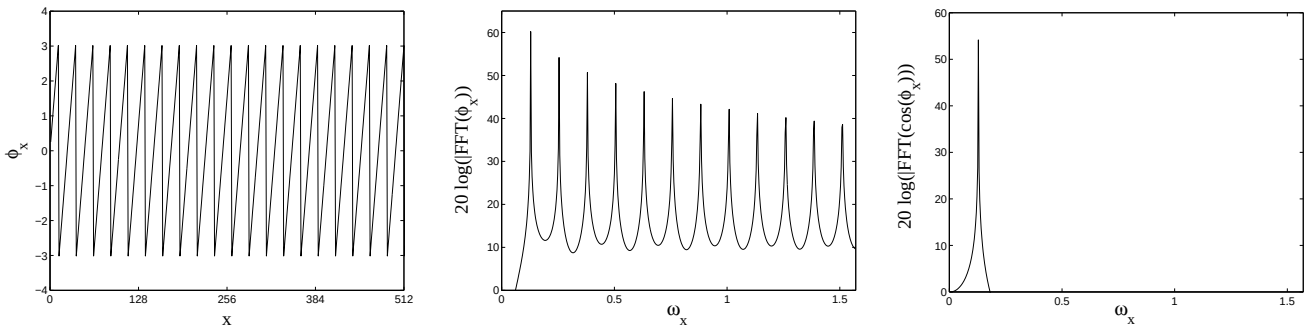

(a) (b) (c)

Figure 4.13: Example of an ideal one-dimensional interferometric phase with a 25-pixel period. (a) Wrapped interferometric phase ϕ_x. (b) Fourier transform amplitude of ϕ_x. (c) Fourier transform amplitude of $\cos(\phi_x)$.

For a one-dimensional signal, by considering Eq. (4.36), the true interferometric phasor can be modelled as follows

$$e^{j\phi_x[m]} = e^{j\frac{2\pi}{N}m} = \cos\left(\frac{2\pi}{N}m\right) + j\sin\left(\frac{2\pi}{N}m\right). \tag{4.37}$$

[2] $N > 2$

This model can be easily extended to the two-dimensional case by assuming the interferometric phase to be separable [174]. In this case, considering m and n as the two spatial coordinates, the interferometric phase can be obtained as $\phi_x[m,n] = \phi_x^1[m] + \phi_x^2[n]$. Therefore, the interferometric phasor is obtained as

$$e^{j\phi_x[m,n]} = e^{j\frac{2\pi}{N_m}m} e^{j\frac{2\pi}{N_n}n} = \left[\cos\left(\frac{2\pi}{N_m}m\right) + j\sin\left(\frac{2\pi}{N_m}m\right)\right]\left[\cos\left(\frac{2\pi}{N_n}n\right) + j\sin\left(\frac{2\pi}{N_n}n\right)\right]. \quad (4.38)$$

The quantities $2\pi/N_m$ and $2\pi/N_n$ denote the signal slopes, or Wavenumber Shifts in each spatial dimension.

As mentioned previously, the interferometric phasor model attempts to consider only the topographic component of the interferometric phase. But, as it has been emphasized at the introduction, the main advantage a SAR systems offers is precisely the capability to obtain spatial details. Therefore, it seems that there is a contradiction between the simplicity of the proposed model and the complexity of the signal being modelled. On the one hand, the simplicity of the model for the true interferometric phasor is precisely what allows the interferometric phasor noise model to be modelled in the wavelet domain. On the other hand, the impossibility of the model to consider spatial details is overcome by the capability of the wavelet transform to consider and to represent these details.

4.3.2 One-dimensional Wavelet Interferometric Phasor Noise Model

Combining the true interferometric phasor model, Eq. (4.37), with the model for the measured interferometric phasor, Eqs. (4.25) and (4.26), it follows

$$\Re\{e^{j\phi}\}[m] = N_c\cos\left(\frac{2\pi}{N}m\right) + v_c \quad (4.39)$$

$$\Im\{e^{j\phi}\}[m] = N_c\sin\left(\frac{2\pi}{N}m\right) + v_s. \quad (4.40)$$

Eqs. (4.39) and (4.40) represent the departure point to define a one-dimensional interferometric phasor noise model at the wavelet domain. Until now, it has been assumed that the sole term containing useful information is the true interferometric phasor $\exp(j2\pi m/N)$. Now, the modulated coherence term $N_c\exp(j2\pi m/N)$ is considered as useful signal. The reason which explains this change is that the wavelet transform will make possible to obtain directly the parameter N_c, which has been shown to be proportional to the coherence $|\rho|$, see Section 4.2.1.

The DWT of a one-dimensional signal is obtained by recursively applying a two-branch filter bank at the low-frequency branch, see Section 3.3.4 at Chapter 3, known as Mallat algorithm. At the wavelet scale 2^j, two sets of coefficients are available. The first set, $\{a_j\}_{j\in\mathbb{Z}}$, contains the coarse approximation coefficients, which represent a low-pass version of the original signal at the frequency interval $\omega \in [-2^{-j}\pi, 2^{-j}\pi)$. The second set, denoted by $\{d_j\}_{j\in\mathbb{Z}}$, is the set of wavelet coefficients which contain information about the original signal at the frequency interval $\omega \in [-2^{j-1}\pi, -2^{-j}\pi)\cup[2^{-j}\pi, 2^{j-1}\pi)$. The iterative process to obtain these sets of coefficients is shown at Fig. 4.14. In each case the equivalent filter is also given.

The properties of the wavelet coefficients depend directly on the wavelet filters h, g employed to calculate the DWT with the Mallat algorithm. Therefore, in order to be independent of the wavelet filter, an idealization of the transformation process is assumed by considering the Shannon family of wavelets [169]. This family leads to the following bank of filters

$$h(\omega) = \begin{cases} \sqrt{2} & \omega \in [-\pi/2, \pi/2) \\ 0 & \text{otherwise} \end{cases} \quad (4.41)$$

$$g(\omega) = \begin{cases} \sqrt{2} & \omega \in [-\pi, -\pi/2)\cup[\pi/2, \pi) \\ 0 & \text{otherwise} \end{cases} \quad (4.42)$$

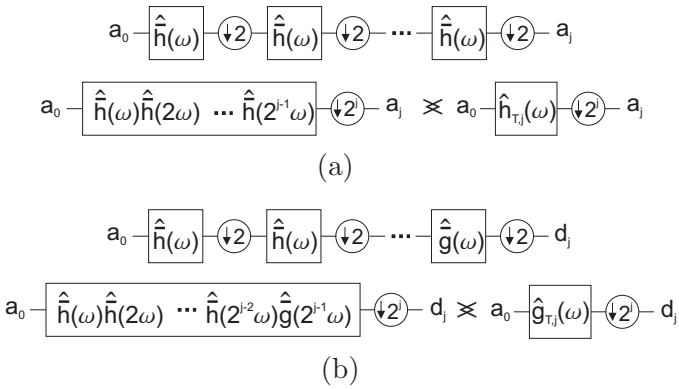

Figure 4.14: Equivalent iterated filters for the one-dimensional DWT at the wavelet scale 2^j. (a) Iteration process to derive the residue coefficients $\{a_j\}_{j\in\mathbb{Z}}$ and the equivalent filter, $\widehat{h}_{T,j}(\omega)$. (b) Iteration process to derive the wavelet coefficients $\{d_j\}_{j\in\mathbb{Z}}$ and the equivalent filter, $\widehat{g}_{T,j}(\omega)$. In each case, the index $_{T,j}$ refers to the equivalent filter response at the scale 2^j.

where $h(\omega)$ and $g(\omega)$ refer, respectively, to a low-pass and a high-pass filter. These filters represent an idealization of the frequency behavior of any wavelet filter, described by Eqs. (3.37), (3.38), (3.48) and (3.49) at Chapter 3, for orthogonal wavelets.

Modulated Coherence Transformation

The DWT of the modulated coherence term, $N_c \exp(j2\pi m/N)$, is now obtained. The wavelet transform of this phasor depends mainly on the value of the frequency $2\pi/N$, since it determines in which wavelet scale the transformed modulated coherence term is contained.

First, the case in which the Wavenumber Shift frequency $2\pi/N \in [-2^{-j}\pi, 2^{-j}\pi)$, i.e., it is concentrated at a coarse approximation band, is considered. For the particular wavelet scale 2^j, the coarse approximation coefficients $\{a_j\}_{j\in\mathbb{Z}}$ are non-zero, whereas the wavelet coefficients $\{d_{j'}\}_{j'\in\mathbb{Z}}$ for $j' \leq j$ are zero. Since the Shannon filters remove aliasing frequencies [23], the coarse approximation coefficients, assuming the equivalent filter introduced at Fig. 4.14a, are obtained at the frequency domain as [141]

$$\widehat{a}_j(\omega) = \frac{1}{2^j}\widehat{h}_{T,j}\left(\frac{\omega}{2^j}\right)\widehat{a}_0\left(\frac{\omega}{2^j}\right). \tag{4.43}$$

By considering the low-pass frequency Shannon filter, Eq. (4.41), the equivalent low-pass filter has the frequency response

$$\widehat{h}_{T,j}(\omega) = \sqrt{2}^j \mathbf{1}_{[-2^{-j}\pi, 2^{-j}\pi)} \tag{4.44}$$

where $\mathbf{1}_{[a,b)}$ represents the boxcar function, which equals one within the interval $\omega \in [a, b)$ and zero otherwise. The signal $a_0[m] = N_c \cos(2\pi m/N)$ represents the real part of the true interferometric phasor, whose Fourier transform $\widehat{a}_0(\omega)$ is

$$\widehat{a}_0(\omega) = \frac{N_c}{2}\left[\delta\left(\omega + \frac{2\pi}{N}\right) + \delta\left(\omega - \frac{2\pi}{N}\right)\right]. \tag{4.45}$$

By introducing Eqs. (4.44) and (4.45) into Eq. (4.43) and calculating the inverse Fourier transform of it, one can prove that the coarse approximation coefficients real part has the expression

$$\Re\{a_j[m]\} = \sqrt{2}^j N_c \cos\left(2^j \frac{2\pi}{N} m\right). \tag{4.46}$$

In a similar way, it can be demonstrated that the coarse approximation coefficients imaginary part follows the expression

$$\Im\{a_j[m]\} = \sqrt{2}^j N_c \sin\left(2^j \frac{2\pi}{N} m\right). \tag{4.47}$$

The second case of interest corresponds to those situations in which the Wavenumber Shift frequency has a value making $2\pi/N \in [-2^{-j+1}\pi, -2^{-j}\pi) \cup [2^{-j}\pi, 2^{-j+1}\pi)$, that is, it is contained in a wavelet band. In this situation, the coefficients $\{d_j\}_{j\in\mathbb{Z}}$ have a value different from zero, whereas the coefficients $\{a_j\}_{j\in\mathbb{Z}}$ and $\{d_{j'}\}_{j'\in\mathbb{Z}}$ for $j' < j$ are zero. The wavelet coefficients $\{d_j\}_{j\in\mathbb{Z}}$ are obtained with the equivalent processing chain depicted at Fig. 4.14b, hence, presenting a slightly different behavior with respect to the coarse approximation coefficients. First of all, the iterated equivalent filter, denoted by $\widehat{g}_{T,j}(\omega)$, considering wavelet Shannon filters, has the expression

$$\widehat{g}_{T,j}(\omega) = \sqrt{2}^{j}\mathbf{1}_{\omega\in[-2^{-j+1}\pi,-2^{-j}\pi)\cup[2^{-j}\pi,2^{-j+1}\pi)}. \tag{4.48}$$

Therefore, as in the coarse approximation coefficients case, the equivalent filter multiplies the useful signal component by the term $\sqrt{2}^{j}$. On the contrary, the subsampling by 2^j introduces an additional modulation process since its input corresponds to a band-pass signal [141]. Since the Mallat algorithm employed to calculate the DWT performs a dyadic division of the frequency domain, the signal modulation produces also an inversion of the signal spectra [141]. The real part of the wavelet coefficients corresponding to the input signal $N_c\cos(2\pi m/N)$ for $2\pi/N \in [-2^{-j+1}\pi, -2^{-j}\pi) \cup [2^{-j}\pi, 2^{-j+1}\pi)$, have the expression

$$\Re\{d_j[m]\} = \sqrt{2}^{j} N_c \cos\left(2(\pi - 2^{j-1}\frac{2\pi}{N})m\right). \tag{4.49}$$

Equivalently, the imaginary part of the wavelet coefficients corresponding to the DWT of $N_c\sin(2\pi m/N)$ follows

$$\Im\{d_j[m]\} = \sqrt{2}^{j} N_c \sin\left(2(\pi - 2^{j-1}\frac{2\pi}{N})m\right). \tag{4.50}$$

Interferometric Noise Phasor Transformation

In order to determine the noise model for the wavelet interferometric phasor it is necessary to determine also the DWT of the noise terms v_c and v_s in Eqs. (4.39) and (4.40). These random processes, as well as their respective DWTs, cannot be characterized by deterministic expressions. Therefore, the analysis is performed by considering their respective spectral density functions.

At Section 4.2, a complete characterization of the first and second moments for v_c and v_s was presented. Therefore, by assuming non-correlated white noises, their respective spectral density functions are

$$G_{v_cv_c}(\omega) = \sigma^2_{v_c}\mathbf{1}_{[-\pi,\pi)} \tag{4.51}$$
$$G_{v_sv_s}(\omega) = \sigma^2_{v_s}\mathbf{1}_{[-\pi,\pi)}. \tag{4.52}$$

In the following, v_c^w and v_s^w are referred as the coefficients at the wavelet domain corresponding to the DWTs of the noise terms v_c and v_s, respectively. As it has been performed for the useful signal term, the characteristics of these transformed noises are analyzed both, for the coarse approximation and the wavelet bands, since both bands are characterized by different processing chains.

The first case concerns the analysis of the interferometric phase noise terms for the coarse approximation band at a given wavelet scale 2^j. The coarse approximation coefficients, before the downsampling process, are obtained as the product of the input signal with the equivalent low-pass filter $\widehat{h}_{T,j}(\omega)$. Therefore, considering $\widehat{v}'_c(\omega)$ the product of $\widehat{v}_c(\omega)$ with the filter $\widehat{h}_{T,j}(\omega)$, the spectral density function of $\widehat{v}'_c(\omega)$ at the coarse approximation band of the wavelet scale 2^j, has the expression

$$G_{v'_cv'_c}(\omega) = G_{v_cv_c}(\omega)|\widehat{h}_{T,j}(\omega)|^2 = \sigma^2_{v_c}2^j\mathbf{1}_{[-2^{-j}\pi,2^{-j}\pi)}. \tag{4.53}$$

Since $E\{v_c\} = 0$, but also, due to the fact that the wavelet coefficients have, by definition, a mean equal to zero, see Eq. (3.17), the variance of v'_c can be derived as follows

$$\sigma^2_{v'_c} = \frac{1}{2\pi}\int_{-\pi}^{\pi} G_{v'_cv'_c}(\omega)\,\mathrm{d}\omega = \frac{1}{2\pi}\int_{-\pi}^{\pi}\sigma^2_{v_c}2^j\mathbf{1}_{[-2^{-j}\pi,2^{-j}\pi)}\,\mathrm{d}\omega = \sigma^2_{v_c}. \tag{4.54}$$

The process after the downsampling, referred as v_c^w, due to the equivalence $E\{a_j^2\} = E\{v_c^{w\,2}\} = E\{v_c'^{\,2}\}$, is a random process with the same variance as the input process v_c. By considering the decorrelation properties of the DWT [23], it can be assumed that the noise term v_c^w has, therefore, the following spectral density function

$$G_{v_c^w v_c^w}(\omega) = \sigma_{v_c}^2 \mathbf{1}_{[-\pi,\pi)}. \tag{4.55}$$

Equally, the spectral density function of v_s^w, which corresponds to the coarse approximation coefficients at the wavelet scale 2^j of the noise term v_s, has the expression

$$G_{v_s^w v_s^w}(\omega) = \sigma_{v_s}^2 \mathbf{1}_{[-\pi,\pi)}. \tag{4.56}$$

For a wavelet band, the process to derive the expressions of $G_{v_c^w v_c^w}(\omega)$ and $G_{v_s^w v_s^w}(\omega)$ is equivalent to the case of the coarse approximation band, but considering the band-pass filter $\widehat{g}_{T,j}(\omega)$ instead of the low-pass filter $\widehat{h}_{T,j}(\omega)$. The spectral density function at the output of the filter $\widehat{g}_{T,j}(\omega)$ corresponds to the spectral density function of a band-pass signals. If the noise term v_c is now considered, the spectral density function of the signal at the filter's output v_c' follows

$$G_{v_c' v_c'}(\omega) = G_{v_c v_c}(\omega)\,|\widehat{g}_{T,j}(\omega)|^2 = \sigma_{v_c}^2 2^j \mathbf{1}_{[-2^{-j+1}\pi,-2^{-j}\pi)\cup[2^{-j}\pi,2^{-j+1}\pi)}. \tag{4.57}$$

By integrating Eq. (4.57), it can be found that also in this case $\sigma_{v_c'}^2 = \sigma_{v_c}^2$. Despite the downsampling process introduces a modulation, the equivalence $E\{d_j^2\} = E\{v_c^{w\,2}\} = E\{v_c'^{\,2}\}$ remains valid. Consequently, the spectral density functions of the noise terms v_c^w and v_s^w at any wavelet band, at any wavelet scale 2^j, are

$$G_{v_c^w v_c^w}(\omega) = \sigma_{v_c}^2 \mathbf{1}_{[-\pi,\pi)} \tag{4.58}$$

$$G_{v_s^w v_s^w}(\omega) = \sigma_{v_s}^2 \mathbf{1}_{[-\pi,\pi)}. \tag{4.59}$$

As it will be demonstrated later in this chapter, the wavelet transform affects the distribution of the noise terms v_c and v_s. But, the most interesting results is that, despite the pdfs are changed, the power of the noise terms v_c^w and v_s^w remains the same as the power of the original domain noise terms, v_c and v_s.

The introduction of a simple model for the true interferometric phasor, see Section 4.3.1, has made possible to derive a noise model for the interferometric phasor at the wavelet domain. As it has been demonstrated, the interferometric phasor's behavior at the scale dimension is determined by the Wavenumber Shift. If the value of the Wavenumber Shift is within the frequency range of a coarse approximation band, for a given number of wavelet scales, the coarse approximation coefficient's phase contains a coarse and downsampled version of the original interferometric phase ϕ_x. On the contrary if the Wavenumber Shift presents a value in the frequency range of a wavelet band, the phase of the wavelet coefficients contain a band-pass filtered, downsampled and frequency inverted version of the original interferometric phase ϕ_x, as a consequence of the band-pass signal downsampling. Independently of the position at the scale dimension, the modulated coherence term is multiplied by $\sqrt{2}^j$, which is induced by the wavelet transformation process. It has been also presented that the DWT does not change the power of the additive noise terms v_c^w and v_s^w, despite their pdfs do. As the DWT is a linear process, the DWT of the interferometric phasor at the original domain, Eqs. (4.39) and (4.40), has the following expression for the complex coarse approximation coefficients

$$a_j[m] = \sqrt{2}^j N_c \exp\left(\mathbf{j} 2^j \frac{2\pi}{N} m\right) + (v_c^w + \mathbf{j} v_s^w) \tag{4.60}$$

whereas the complex wavelet coefficients have the expression

$$d_j[m] = \sqrt{2}^j N_c \exp\left(\mathbf{j} 2(\pi - 2^{j-1}\frac{2\pi}{N})m\right) + (v_c^w + \mathbf{j} v_s^w). \tag{4.61}$$

From these expressions it is possible to observe that the DWT increases the modulated coherence amplitude and maintains the variance of the additive noise terms. Consequently, it can be clearly concluded that the transformation process improves the quality of the useful signal component [169]. This improvement can be measured by the Signal to Noise Ratio (SNR), which measures the ratio between the useful signal power and the noise power [48]. For a coarse approximation band, considering the Wavenumber shift $2\pi/N$ to be within the frequency range of it, the SNR is

$$\mathrm{SNR}_{a_j} = \frac{E\{|\sqrt{2}^j N_c e^{\mathbf{j}2^j \frac{2\pi}{N} m}|^2\}}{E\{|v_c^w + \mathbf{j}v_s^w|^2\}} = 2^j \frac{N_c^2}{\sigma^2_{v_c^w} + \sigma^2_{v_s^w}} = 2^j \frac{N_c^2}{\sigma^2_{v_c} + \sigma^2_{v_s}}. \tag{4.62}$$

The SNR for a signal located at a wavelet band has the same expression

$$\mathrm{SNR}_{d_j} = 2^j \frac{N_c^2}{\sigma^2_{v_c} + \sigma^2_{v_s}}. \tag{4.63}$$

To sum up, the wavelet transformation process increases the SNR of the modulated coherence term at the wavelet domain for a fixed value of N_c (a fixed coherence value), in such a way that the larger the number of wavelet scales, the larger the improvement.

4.3.3 Two-dimensional Wavelet Interferometric Phasor Noise Model

SAR imagery consist in two-dimensional signals. Therefore, the one-dimensional interferometric phasor noise model at the wavelet domain has to be extended for two-dimensional signals. This extension has also to consider the particularities of the process employed to obtain the DWT, in this case, the two-dimensional Mallat algorithm, see Section 3.3.5. This section, hence, regards the definition of the two-dimensional noise model for the interferometric phasor at the wavelet domain, whose complex argument consists of a two-dimensional interferometric phase $\phi_x[m,n]$. This new noise model is derived by considering an ideal two-dimensional interferometric phasor signal, already introduced by Eq. (4.38), since it allows to characterize, in a very efficient way, the interferometric phasor within the wavelet domain. Finally, the noise model will be generalized by considering an arbitrary interferometric phase.

A complete description of the measured interferometric phasor at the original domain is obtained by combining the separable two-dimensional true interferometric phasor model, Eq. (4.38), with the interferometric phasor noise model Eqs. (4.25) and (4.26), from where it follows

$$\Re\{e^{j\phi}\}[m,n] = N_c \cos\left(\frac{2\pi}{N_m}m + \frac{2\pi}{N_n}n\right) + v_c \tag{4.64}$$

$$\Im\{e^{j\phi}\}[m,n] = N_c \sin\left(\frac{2\pi}{N_m}m + \frac{2\pi}{N_n}n\right) + v_s. \tag{4.65}$$

In this case, the parameter N_c, as well as the additive noise terms v_c and v_s refer to two-dimensional signals.

The two-dimensional DWT is calculated by applying, in a separable way, the one-dimensional DWT to each one of the input signal dimensions. The difference with the one-dimensional DWT is that, at any wavelet scale 2^j, four sets of transformed coefficients, instead of two, are available. The first set, $\{a_j\}_{j\in\mathbb{Z}}$, contains a coarse approximation of the input signal. On the contrary, the three sets of wavelet coefficients, denoted by $\{d_j^H, d_j^V, d_j^D\}_{j\in\mathbb{Z}}$, contain details of the input signal at different ranges of spatial frequencies. In this case, the Shannon family of wavelet filters is also employed as a way to derive a general expression for the interferometric phasor noise model in the wavelet domain, whatever the filter employed to calculate the DWT. Fig. 4.15 presents an scheme of the two-dimensional DWT. At each final branch, at a given wavelet scale 2^j, the corresponding equivalent iterated filter is also depicted.

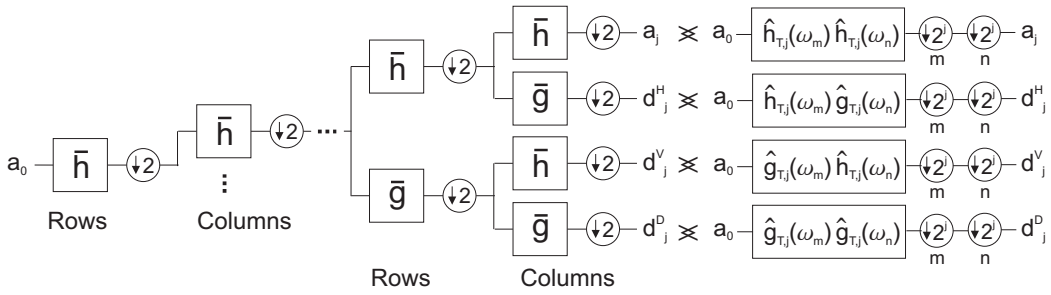

Figure 4.15: Equivalent iterated filters for the two-dimensional DWT at the wavelet scale 2^j. The index m refers to the row dimension, whereas n refers to the column dimension.

Before to obtain the noise model at the wavelet domain for the interferometric phasor, the following conventions are included. With respect to the ranges of spatial frequencies associated with the wavelet filters and the wavelet scales, the next notation is introduced

$$\omega_{j,k}^{\mathcal{L}} = \omega_k \in [-2^{-j}\pi, 2^{-j}\pi) \tag{4.66}$$

$$\omega_{j,k}^{\mathcal{B}} = \omega_k \in [-2^{-j+1}\pi, -2^{-j}\pi) \cup [2^{-j}\pi, 2^{-j+1}\pi) \tag{4.67}$$

where j refers to the wavelet scale coordinate, $k \in \{m, n\}$ to the spatial coordinates, and $\mathcal{L}$ and $\mathcal{B}$ denote low and band-pass frequencies respectively. On the other hand, the equivalent responses of the iterated filters involved in the process to calculate the two-dimensional DWT are employed with the following notation, see Fig. 4.15

$$\widehat{h}_{T,j}(\omega_m, \omega_n) = \widehat{h}_{T,j}(\omega_m)\widehat{h}_{T,j}(\omega_n) = 2^j \mathbf{1}_{\omega_{j,m}^{\mathcal{L}}} \mathbf{1}_{\omega_{j,n}^{\mathcal{L}}} \tag{4.68}$$

$$\widehat{g}_{T,j}^{H}(\omega_m, \omega_n) = \widehat{h}_{T,j}(\omega_m)\widehat{g}_{T,j}(\omega_n) = 2^j \mathbf{1}_{\omega_{j,m}^{\mathcal{L}}} \mathbf{1}_{\omega_{j,n}^{\mathcal{B}}} \tag{4.69}$$

$$\widehat{g}_{T,j}^{V}(\omega_m, \omega_n) = \widehat{g}_{T,j}(\omega_m)\widehat{h}_{T,j}(\omega_n) = 2^j \mathbf{1}_{\omega_{j,m}^{\mathcal{B}}} \mathbf{1}_{\omega_{j,n}^{\mathcal{L}}} \tag{4.70}$$

$$\widehat{g}_{T,j}^{D}(\omega_m, \omega_n) = \widehat{g}_{T,j}(\omega_m)\widehat{g}_{T,j}(\omega_n) = 2^j \mathbf{1}_{\omega_{j,m}^{\mathcal{B}}} \mathbf{1}_{\omega_{j,n}^{\mathcal{B}}} \tag{4.71}$$

where the responses $\widehat{h}_{T,j}(\omega)$ and $\widehat{g}_{T,j}(\omega)$, corresponding to the Shannon wavelet filters, represent the one-dimensional responses at each frequency dimension, ω_m and ω_n. Additionally, the responses of the three wavelet filters, $\widehat{g}_{T,j}^{H}(\omega_m, \omega_n)$, $\widehat{g}_{T,j}^{V}(\omega_m, \omega_n)$ and $\widehat{g}_{T,j}^{D}(\omega_m, \omega_n)$ are expressed by $\widehat{g}_{T,j}^{l}(\omega_m, \omega_n)$, where $l \in \{H, V, D\}$.

Two-dimensional Modulated Coherence Phasor Transform

From Eqs. (4.64) and (4.65), which consist of the real and imaginary parts of the interferometric phasor in the original domain, the first addend is taken, as it has been assumed for the one-dimensional case, as the useful signal term. Consequently, these signals are considered the approximation coefficients $a_0[m, n]$, at the wavelet scale 2^0 [23].

The first case to analyze is produced in those situations in which, given a wavelet scale 2^j, the Wavenumber Shift at the dimension ω_m is within the range frequency $\omega_{j,m}^{\mathcal{L}}$ and the Wavenumber Shift at the dimension ω_n is also in a low frequency range, that is $\omega_{j,n}^{\mathcal{L}}$. This produces the coefficients $a_j[m, n]$ to contain information from the input true interferometric phasor, whereas the wavelet coefficients $d_{j'}^{k}[m, n]$, for $k \in \{H, V, D\}$ and $j' \leq j$ are zero. The coarse approximation coefficients are obtained by filtering the input signal $a_0[m, n]$ with the iterated two-dimensional low-pass filter $\widehat{h}_{T,j}(\omega_m, \omega_n)$ followed by a downsampling by 2^j in each dimension, as shown in Fig. 4.15. The input signal, defined as the product of the true interferometric phasor by N_c, is modelled as a separable function, i.e. $a_0[m, n] = a_0^1[m]a_0^2[m]$, see Eq. (4.38). Therefore, since the wavelet filter, as well as the input signal are separable functions,

the value of the coarse approximation coefficients, at the wavelet scale 2^j, is obtained at the frequency domain as

$$\widehat{a}_j(\omega_m,\omega_n)=\frac{1}{2^j}\frac{1}{2^j}\widehat{h}_{T,j}\left(\frac{\omega_m}{2^j}\right)\widehat{h}_{T,j}\left(\frac{\omega_n}{2^j}\right)\widehat{a}_0^1\left(\frac{\omega_m}{2^j}\right)\widehat{a}_0^2\left(\frac{\omega_n}{2^j}\right). \tag{4.72}$$

The final expression of Eq. (4.72) can be obtained as a simple extension of the results obtained for the one-dimensional case. Hence, the inverse Fourier transform of Eq. (4.72) is simply the product of the inverse Fourier transforms at each spatial dimension. Considering the true interferometric phase model Eq. (4.38) multiplied by the parameter N_c as the true interferometric phasor, the inverse Fourier transform of Eq. (4.72), which corresponds to the coarse approximation coefficients, is [169]

$$a_j[m,n]=2^jN_c\exp\left(\mathbf{j}2^j\frac{2\pi}{N_m}m\right)\exp\left(\mathbf{j}2^j\frac{2\pi}{N_n}n\right). \tag{4.73}$$

Now, the interest is on obtaining the expression for the wavelet coefficients $d_j^l[m,n]$ for $l\in\{H,V,D\}$. In those situations in which the Wavenumber Shifts at each spatial dimension, for a given wavelet scale 2^j, have values producing the two-dimensional Wavenumber Shift to be inside the frequency range of one of the three wavelet bands at the scale 2^j, Eqs. (4.69), (4.70) and (4.71), the wavelet coefficients corresponding to this band contain information about the original signal. On the contrary, the coarse approximation coefficients $a_j[m,n]$, the wavelet coefficients corresponding to the remaining wavelet bands at the same wavelet scale 2^j, and the wavelet coefficients $d_{j'}^l[m,n]$ for $l\in\{H,V,D\}$ and $j'<j$, are zero. For an arbitrary wavelet band, the Fourier transform of the wavelet coefficients $d_j^l[m,n]$, considering separability for the input signal, has the expression

$$\widehat{d}_j^l(\omega_m,\omega_n)=\frac{1}{2^j}\frac{1}{2^j}\widehat{g}_{T,j}^l\left(\frac{\omega_m}{2^j},\frac{\omega_m}{2^j}\right)\widehat{a}_0^1\left(\frac{\omega_m}{2^j}\right)\widehat{a}_0^2\left(\frac{\omega_n}{2^j}\right) \tag{4.74}$$

where $l\in\{H,V,D\}$. As in this case also, all the components are separable signals, the expression of the wavelet coefficients at the wavelet band $d_j^l[m,n]$ can be obtained by employing the results deduced for the one-dimensional case. In order to derive a compact expression for the wavelet coefficients, the following convention for the phase is assumed

$$\phi_x^{\mathcal{L}}[p] = 2^j\frac{2\pi}{N_p}p \tag{4.75}$$

$$\phi_x^{\mathcal{B}}[p] = 2\left(\pi-2^{j-1}\frac{2\pi}{N_p}\right)p. \tag{4.76}$$

Therefore, the expression of the wavelet coefficients at any wavelet band $l\in\{H,V,D\}$ and wavelet scale 2^j follows [169]

$$d_j^l[m,n]=2^jN_c\exp(\mathbf{j}\phi_x^{l_1}[m])\exp(\mathbf{j}\phi_x^{l_2}[n]) \tag{4.77}$$

where

$$l=H \;\Rightarrow\; l_1=\mathcal{L},\; l_2=\mathcal{B} \tag{4.78}$$

$$l=V \;\Rightarrow\; l_1=\mathcal{B},\; l_2=\mathcal{L} \tag{4.79}$$

$$l=D \;\Rightarrow\; l_1=\mathcal{B},\; l_2=\mathcal{B}. \tag{4.80}$$

A brief comparison between the expressions of the two-dimensional coefficients at the wavelet domain, Eqs. (4.73) and (4.77), with the equivalent expressions for the one-dimensional case, Eqs. (4.46), (4.47), (4.49) and (4.50), shows the complete similarity between them, except for the fact that the two-dimensional wavelet transform introduces a larger multiplying factor, 2^j instead of $\sqrt{2}^j$.

Two-Dimensional Interferometric Phasor Noise Transform

In order to derive the complete noise model for the interferometric phasor at the wavelet domain, it is also necessary to obtain the two-dimensional DWT of the additive noise terms v_c and v_s at Eqs. (4.64) and

(4.65). Both noise components are assumed to be spatially non-correlated terms. Hence, their spectral density functions are

$$G_{v_c v_c}(\omega_m, \omega_n) = \sigma^2_{v_c} \mathbf{1}_{\omega_m \in [-\pi,\pi)} \mathbf{1}_{\omega_n \in [-\pi,\pi)} \quad (4.81)$$

$$G_{v_s v_s}(\omega_m, \omega_n) = \sigma^2_{v_s} \mathbf{1}_{\omega_m \in [-\pi,\pi)} \mathbf{1}_{\omega_n \in [-\pi,\pi)}. \quad (4.82)$$

The procedure to characterize these noise components in the wavelet domain, also denoted by v_c^w and v_s^w, is very similar to the one employed for the one-dimensional case. In the following, v'_c and v'_s denote the signals at the output of the equivalent iterated filters presented in Fig. 4.15 for the signals v_c and v_s respectively.

The noise power at the coarse approximation band, given by the coefficients $a_j[m,n]$, is obtained by integrating the spectral density functions corresponding to the filtered additive noise terms v'_c and v'_s. For the real part case v'_c, the corresponding spectral density function has the expression

$$G_{v'_c v'_c}(\omega_m, \omega_n) = G_{v_c v_c}(\omega_m, \omega_n) |\widehat{h}_{T,j}(\omega_m, \omega_n)|^2 = \sigma^2_{v_c} 2^{2j} \mathbf{1}_{\omega^{\mathcal{L}}_{j,m}} \mathbf{1}_{\omega^{\mathcal{L}}_{j,n}}. \quad (4.83)$$

The noise power corresponding to it, v'_c, is found by integrating the previous spectral density function

$$\begin{aligned} \sigma^2_{v'_c} &= \frac{1}{2\pi}\frac{1}{2\pi} \int_{-\pi}^{\pi}\int_{-\pi}^{\pi} G_{v_c^{w\prime} v_c^{w\prime}}(\omega_m, \omega_n)\, \mathrm{d}\omega_m\, \mathrm{d}\omega_n \\ &= \frac{1}{2\pi}\frac{1}{2\pi} \int_{-\pi}^{\pi}\int_{-\pi}^{\pi} \sigma^2_{v_c} 2^{2j} \mathbf{1}_{\omega^{\mathcal{L}}_{j,m}} \mathbf{1}_{\omega^{\mathcal{L}}_{j,n}}\, \mathrm{d}\omega_m\, \mathrm{d}\omega_n = \sigma^2_{v_c}. \end{aligned} \quad (4.84)$$

Since the downsampling process at both dimensions of the input signal does not alter the noise variance, one can conclude from the result obtained at Eq. (4.84), that the spectral density function of the additive noise terms, for a coarse approximation band at the wavelet domain, considering the decorrelation properties of the DWT, have the expressions

$$G_{v_c^w v_c^w}(\omega_m, \omega_n) = \sigma^2_{v_c} \mathbf{1}_{\omega_m \in [-\pi,\pi)} \mathbf{1}_{\omega_n \in [-\pi,\pi)} \quad (4.85)$$

$$G_{v_s^w v_s^w}(\omega_m, \omega_n) = \sigma^2_{v_s} \mathbf{1}_{\omega_m \in [-\pi,\pi)} \mathbf{1}_{\omega_n \in [-\pi,\pi)}. \quad (4.86)$$

Since the noise terms v_c and v_s have white spectral density functions, see Eqs. (4.81) and (4.82), all the coefficients at the wavelet domain are affected by noise whatever the useful signal content. Therefore, also the transformed additive noise terms v_c^ω and v_s^ω properties have to be investigated for the wavelet coefficients $d_j^l[m,n]$, for $l \in \{H, V, D\}$. All the wavelet filters $\widehat{g}^l_{T,j}(\omega_m, \omega_n)$, for a given wavelet scale 2^j, have the same amplitude, equal to 2^j, and occupy the same area over the two-dimensional frequency space, which equals to $(2\pi/2^j)^2$. Considering these values, the variance of the real part additive noise term, v_c, after filtering it with any iterated wavelet filter, equals to

$$\sigma^2_{v'_c} = \frac{1}{2\pi}\frac{1}{2\pi} \int_{-\pi}^{\pi}\int_{-\pi}^{\pi} G_{v_c^w v_c^w}(\omega_m, \omega_n) \widehat{g}^l_{T,j}(\omega_m, \omega_n)\, \mathrm{d}\omega_m\, \mathrm{d}\omega_n = \sigma^2_{v_c} \quad (4.87)$$

for $l \in \{H, V, D\}$. This result is also valid for the imaginary part of the additive noise v_s. Consequently, at any wavelet band, the spectral density at the wavelet domain, corresponds also to Eqs. (4.85) and (4.86).

As a brief conclusion of this section, it has been demonstrated that also in the case of the two-dimensional case, the DWT does not alter the variance of the additive noise terms of the interferometric phasor noise model, despite, as it will be presented, their distributions are.

From the results obtained in the previous two sections, one can finally derive the expression for the two-dimensional interferometric phasor in the wavelet domain, whose model, for the original or spatial

domain is given by Eqs. (4.64) and (4.65). Therefore, the complex coarse approximation coefficients behavior, at any wavelet scale 2^j, are described by the following model

$$a_j[m,n] = 2^j N_c \exp\left(\mathbf{j}\frac{2\pi}{N_m}m\right)\exp\left(\mathbf{j}\frac{2\pi}{N_n}n\right) + (v_c^w + \mathbf{j}v_s^w) \tag{4.88}$$

where the two-dimensional additive noises v_c^w and v_c^w are completely described by the spectral density functions given by Eqs. (4.85) and (4.86). With respect to the expression of the noise model for the wavelet coefficients, the different content of spatial frequencies at each one of the three possible wavelet bands has to be considered. Taking the convention employed to describe the frequency content at the wavelet domain, Eqs. (4.75) and (4.76), the discrete complex wavelet coefficients have the following noise model expression

$$d_j^l[m,n] = 2^j N_c \exp(\mathbf{j}\phi_x^{l_1}[m])\exp(\mathbf{j}\phi_x^{l_2}[n]) + (v_c^w + \mathbf{j}v_s^w) \tag{4.89}$$

where l refers to H, V or D respectively for the horizontal, vertical and diagonal wavelet detail bands.

As it has been assumed throughout this section, the first additive term of the noise model Eqs. (4.88) and (4.89), which contains the true interferometric phase information as well as the noise parameter N_c, is taken as useful signal. The effect of the two-dimensional wavelet transform can be quantitatively measured by the Signal to Noise Ratio. If this ratio is calculated for the coarse approximation coefficients, the following value is obtained

$$\mathrm{SNR}_{a_j} = \frac{E\{|2^j N_c e^{\mathbf{j}2^j\frac{2\pi}{N_m}m} e^{\mathbf{j}2^j\frac{2\pi}{N_n}n}|^2\}}{E\{|v_c^w + \mathbf{j}v_s^w|^2\}} = 2^{2j}\frac{N_c^2}{\sigma_{v_c}^2 + \sigma_{v_s}^2}. \tag{4.90}$$

In the case of the wavelet coefficients $d_j^l[m,n]$, for $l \in \{H,V,D\}$, one can demonstrate that the SNR has the same value

$$\mathrm{SNR}_{d_j^l} = 2^{2j}\frac{N_c^2}{\sigma_{v_c}^2 + \sigma_{v_s}^2}. \tag{4.91}$$

As it can be observed, the two-dimensional DWT increases the SNR by a larger factor than the one-dimensional DWT does. One important conclusion which can be extracted from Eqs. (4.90) and (4.91) is that the improving effect introduced by the two-dimensional DWT does not depend neither on the signal location at the scale dimension nor on its spatial location.

4.4 Generalized Wavelet Interferometric Phasor Noise Model

As it can be observed at a glance, the topography of any natural surface is characterized by being extremely heterogeneous and containing numerous spatial details. These details can be completely natural or, on the contrary, to be man-made structures. The SAR systems spatial resolution, typically in the range of a few meters, makes SAR data to be sensitive to these details. As a result, the interferometric phase difference signal does not only contain the topographic component, but also the information concerning the spatial details. The immediate conclusion which can be extracted from these facts is that the interferometric phase is a complex and very heterogeneous signal.

Within the first part of this chapter, Section 4.2, a general noise model for the measured interferometric phasor has been obtained. This model has allowed to identify how the true interferometric phasor is damaged by noise, without introducing any restriction on the signals to analyze. Subsequently, this model has been employed to obtain a new noise model for the interferometric phasor in the wavelet domain. This model is based, on the contrary, on assuming the interferometric phase to follow a particular signal model, see Section 4.3.1. The two-dimensional interferometric phase $\phi_x[m,n]$ is assumed to be a separable signal. Furthermore, each of its components, $\phi_x^1[m]$ and $\phi_x^2[n]$, are considered sawtooth signals with a given period, and whose values range from $-\pi$ to π. The aim of this model for the interferometric phase has been to represent the topographic component. Beyond the fact that this model represents a

simplification of the reality, it allows to obtain a noise model for the interferometric phasor in the wavelet domain. Therefore, the wavelet noise model for the interferometric phasor has to be judged from two different points of view. On the one hand, its simplicity has made possible to understand the behavior, but also to characterize the measured interferometric phasor in this domain. But, on the other hand, its effectiveness to represent real signals. Consequently, the interferometric phasor noise model in the wavelet domain has to be generalized to consider any interferometric phase.

As shown, the nature of the noise model in the wavelet domain depends clearly on the properties of the interferometric phase ϕ_x, since it determines the position of a given signal feature at the scale or frequency dimension. The low-frequency components of the interferometric phase will appear concentrated on the coarse approximation coefficients $a_j[m,n]$. Those components with higher frequency content will appear at the different wavelet bands $d_j^l[m,n]$, for $l \in \{H,V,D\}$, depending on its spatial frequency nature, in such a way that the higher the frequency content the lower the wavelet scale where they will be concentrated. For the coarse approximation coefficients, the true interferometric phase in the wavelet domain ϕ_x^w contains a coarse version of the true interferometric phase ϕ_x, whereas for the wavelet coefficients it represents a band-filtered and frequency inverted version of ϕ_x. The interferometric phasor noise model expressions at the wavelet domain, Eqs. (4.88) and (4.89), can be merged to obtain a general noise model as follows [169]

$$DWT_{2D}\{e^{\mathbf{j}\phi}\}[j,m,n] = 2^j N_c \exp(\mathbf{j}\phi_x^w) + (v_c^w + \mathbf{j}v_s^w). \tag{4.92}$$

Let's analyze each of the terms within the previous equation. The components v_c^w and v_s^w are additive noise terms for the real and imaginary parts of the coefficients in the wavelet domain. The variances of these noise terms do not depend on the wavelet scale 2^j, being equal to the variances of the noise terms in the original domain, v_c and v_s, respectively. The term ϕ_x^w, which is defined in the following as the *wavelet interferometric phase* [169], contains information about the true interferometric phase ϕ_x. The characteristics of this phase depend on the wavelet band 2^j, but also on the wavelet scale $a_j[m,n]$ or $d_j^l[m,n]$, for $l \in \{H,V,D\}$. Finally, coherence information is included through the parameter N_c. It has to be mentioned that the terms N_c, ϕ_x^w, v_c^w and v_s^w also depend on the spatial coordinates m and n. Therefore, the interferometric information given by $N_c \exp(j\phi_x^w)$ is analyzed, due to the wavelet transform nature, in a space-frequency frame.

The availability of a new noise model for the interferometric phasor in the wavelet domain has made possible to analyze the signal, as well as the noise components, in the wavelet domain. This noise model has been developed for the real and imaginary parts of the coefficients $a_j[m,n]$ and $d_j^l[m,n]$, for $l \in \{H,V,D\}$, at the wavelet domain. But, as it is analyzed in the following, the amplitude and the phase of such coefficients can be related with more physical quantities than the real and imaginary parts are. Some of the results which are going to be presented in the following have been already shown throughout this section. Before to analyze the amplitude and the phase of the coefficients in the wavelet domain, an analysis of these quantities in the space domain is presented. By simple observation of the interferometric phasor noise model, Eq. (4.30), it can be deduced that at the space domain, the phase is just the noisy interferometric phase. The way in which the noise model for the interferometric phasor has been defined determines also that the amplitude is constant and equal to one. Therefore, no information can be extracted from it.

In the wavelet domain, an expression for the intensity of the transformed coefficients can be derived trough the generalized noise model for the interferometric phasor. The expression given by Eq. (4.92) is valid for any transformed coefficient $a_j[m,n]$ or $d_j^l[m,n]$, for $l \in \{H,V,D\}$. In this case, the difference between the coefficients is on the information contained within the term $N_c \exp(j\phi_x^w)$. The expectation of the coefficient intensity at the wavelet domain, considering the useful signal and the noise components

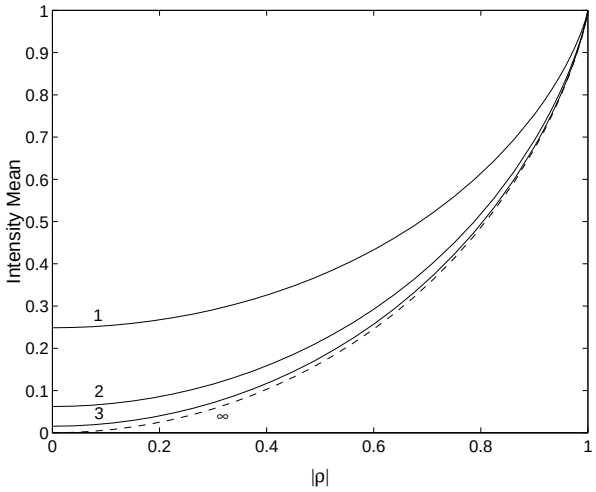

Figure 4.16: Effect of the number of wavelet scales for the DWT on the intensity of the coefficients at the wavelet domain. In this case, the intensity is normalized by 2^{2j}. The numbers indicate the number of wavelets scales j. The infinite indicates an infinite number of scales, hence, the intensity is directly equal to N_c^2.

to be homogeneous, is found to be

$$\begin{aligned} E\left\{\left|DWT_{2D}\{e^{\mathbf{j}\phi}\}\right|^2\right\} &= E\left\{(2^j N_c\cos(\phi_x^w)+v_c^w)^2\right\}+E\left\{(2^j N_c\sin(\phi_x^w)+v_s^w)^2\right\} \\ &= 2^{2j}N_c^2+\sigma_{v_c^w}^2+\sigma_{v_s^w}^2 = 2^{2j}N_c^2+\sigma_{v_c}^2+\sigma_{v_s}^2. \end{aligned} \tag{4.93}$$

The previous equation shows the importance of the information included in the intensity of the coefficients at the wavelet domain. The intensity depends on the variance of the additive noise terms $\sigma_{v_c}^2$ and $\sigma_{v_s}^2$, but also on the parameter N_c^2, which embodies coherence information. The weight of the term N_c^2 compared with the noise variances depends on the wavelet scale 2^j, since it is multiplied by 2^{2j}. The important consequence is that the larger the wavelet scale, the more negligible the noise terms with respect to N_c^2. This effect can be clearly seen in Fig. 4.16, which represents the intensity value normalized by 2^{2j}. What it is surprising from this figure is that for a three-scale DWT, the effect of the additive noise terms can be considered negligible in front of N_c^2, and therefore, the intensity of the transformed coefficients can be directly related with coherence information. This important consequence justifies, therefore, to consider the parameter N_c as a useful signal components despite it is purely generated by the additive noise component of the interferometric phase. Therefore, the wavelet transform, introduces an improvement of the useful signal term, as it has been already shown at Eqs. (4.90) and (4.91), allowing to directly derive coherence information from the signal in the wavelet domain [175].

The analysis of the intensity value of the coefficients at the wavelet domain, Eq. (4.93), needs additional study. Going back, the value of N_c is given by Eq. (4.11), whereas the values of the noise variances $\sigma_{v_c}^2$ and $\sigma_{v_s}^2$ are given by Eq. (4.29). From these expressions, one can observe that they depend on the coherence value $|\rho|$ in such a way that $\sigma_{v_c}^2+\sigma_{v_s}^2 \leq 1$ and $N_c^2+\sigma_{v_c}^2+\sigma_{v_s}^2 = 1$. As mentioned in Chapter 3, one of the main properties of the wavelet transform is its capability to introduce space resolution within the frequency domain. Furthermore, the coefficients in the wavelet domain located at different wavelet scales, are related since they provide information, at different frequency ranges, of the same spatial area [176, 23]. In the case of the Mallat algorithm, a hierarchical relation can be established among the coefficients at different scales, as it can be observed in Fig. 4.17.

Given the intensity value of a coefficient in the wavelet domain, Eq. (4.93), the values of $\sigma_{v_c}^2$ and $\sigma_{v_s}^2$ depend on the coherence of the spatial location described by the wavelet coefficient. The maximum value occurs for zero coherence areas, where $\sigma_{v_c}^2+\sigma_{v_s}^2 = 1$. On the other hand, as given by Eq. (4.92), the term $2^{2j}N_c^2$ corresponds to the intensity of the wavelet interferometric phasor $\exp(j\phi_x^w)$. As a result, the intensity value at the wavelet domain is affected by this phasor, in such a way that the amplitude

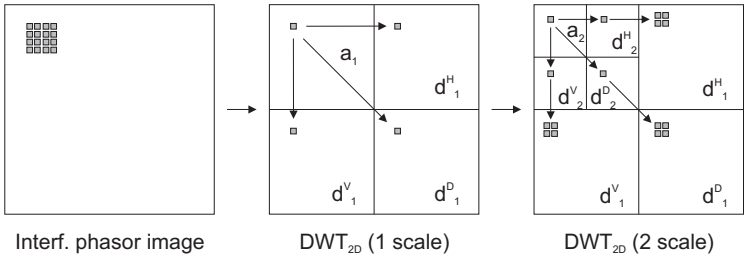

Figure 4.17: Hierarchical relation among the coefficients of the wavelet domain at different wavelet scales, but containing information about the same area of the original image.

$2^j N_c$ is modulated by the component $\exp(j\phi_x^w)$. This effect produces that if a given coefficient in the wavelet domain is in a space-frequency location where interferometric phase exists, its average intensity is equal to $2^{2j}N_c^2 + \sigma_{v_c}^2 + \sigma_{v_s}^2$. On the contrary, the average intensity is only proportional to $\sigma_{v_c}^2 + \sigma_{v_s}^2$, which depends, as explained, on the coherence value.

Summarizing, the intensity of a given wavelet coefficient has two components. The first one depends on the variances of the additive noise terms, in such a way that the lower the coherence the higher the variances. The second components is the intensity of the term $2^j N_c^2 \exp(\mathbf{j}\phi_x^w)$. Therefore, this intensity term has to be understood as a modulated coherence, which is precisely modulated by the interferometric phase ϕ_x^w. Owing to the analysis capabilities of the wavelet theory, one can conclude that it will allow to analyze the interferometric information, both coherence a phase, in a space-frequency frame.

The phase in the wavelet domain ϕ_x^w has been defined as the wavelet interferometric phase. From the generalized model for the interferometric phasor at the wavelet domain, Eq. (4.92), one can extract the expression of the phase component for a given coefficient at the wavelet domain

$$\arg\left\{DWT_{2D}(e^{j\phi})\right\} = \arctan\left(\frac{2^j N_c \sin(\phi_x^w) + v_s^w}{2^j N_c \cos(\phi_x^w) + v_c^w}\right) \tag{4.94}$$

where $\arg\{\cdot\}$ refers to the complex argument or phase. Observing Eq. (4.94), it can be noticed that provided the value $2^j N_c$ to be high enough, the argument of the coefficient is basically the value ϕ_x^w, that is, the original wavelet interferometric phase information. Obviously, the type of information contained in the phase depends on the wavelet band nature. On the other hand, if the value of the parameter $2^j N_c$ is close to zero, the argument of the coefficient is $\arctan(v_s^w/v_c^w)$. Owing to the fact that v_c^w and v_s^w are noise processes, the phase of these coefficients can be consider to contain only noise. Before to conclude this section, it is worthwhile to summarize what has been presented until this point. In Section 4.2, a model for the interferometric phasor in the original domain has been proposed and validated. As shown, this model, by itself, is not very useful since very little information can be extracted from it. The noise model for the interferometric phasor has been transformed to the wavelet domain, where it has been shown that relevant interferometric information can be extracted. Basically speaking, the DWT is able to locate interferometric information, both coherence and phase, in a space-frequency frame. The useful interferometric information at the wavelet domain has to be understood as a *modulated coherence information*. Consequently, the overall behavior of the wavelet domain coefficients can be summarized as follows [169]:

- The position in the scale dimension gives frequency information about the interferometric phase signal.
- The position in the space dimension gives spatial location about the frequency content.
- The coefficient value gives two information in a local space-frequency area. If the intensity has a high value, that is a high value of $2^j N_c$, the phase contains information about topography and coherence information can be extracted from phase. These coefficients are defined as *signal coefficients*. On the contrary, if the intensity is low, that is, N_c is equal to zero, the phase contains only noise. These coefficients are defined as *noise coefficients*.

4.5 Wavelet Interferometric Phasor Statistics

As stated before, Eq. (4.92) represents a noise model for the interferometric phasor in the wavelet domain. This model can be employed for a wide range of data processing techniques, as for instance noise reduction. In many cases, these techniques are also based on the knowledge of the data pdf. This section concerns the definition of a proper statistical model for the interferometric phasor in the wavelet domain, considering the particularities of the transformation process and the signal to transform [177].

The development of the interferometric phasor noise model in the wavelet domain was based on a simple signal model for the true interferometric phasor. Let's ϕ_x an interferometric phase corresponding to a constant slope being described by Eq. (4.38). In the wavelet domain, the transformed terms $\cos(\phi_x^w)$ and $\sin(\phi_x^w)$ are deterministic. In addition, if the coherence is assumed to be constant, the statistical properties of the noise terms v_c and v_s are homogeneous, producing N_c to be also constant. Under these circumstances, the useful signal terms in the wavelet domain, $2^j N_c \exp(\mathbf{j}\phi_x^w)$, is deterministic, being the terms v_c^w and v_s^w the sole components with a random behavior. It has been demonstrated that due to the frequency properties of the measured interferometric phasor, noise affects all the wavelet bands whereas the useful signal term is only concentrated in one scale. This situation allows to analyze noise separately from signal.

The DWT is obtained as the convolution of the input signal with a filter bank. Therefore, the transformed signal can be seen as a weighted sum. By the Central Limit Theorem (CLT) [72], the weighted sum of identically distributed random variables are well approximated by a Gaussian distribution. The noise terms v_c and v_s do not have a Gaussian distribution, but the terms v_c^w and v_s^w, by the CLT, should be approximately zero-mean Gaussian distributed with variance values given by Eqs. (4.21), (4.22) and (4.29), respectively. This distribution is valid for those coefficients which contain only noise. On the contrary, those coefficients affected also by useful signal contain the deterministic term $2^j N_c \exp(\mathbf{j}\phi_x^w)$. Hence, these coefficients can be seen as the addition of a deterministic term plus a zero-mean, complex Gaussian distributed noise. Denoting the real and imaginary parts of a coefficient in the wavelet domain by x and y respectively, and also considering $\sigma = \sigma_{v_c^w} = \sigma_{v_s^w}$, the joint pdf of the real and the imaginary part is

$$p_{x,y}(x,y) = \frac{1}{2\pi\sigma^2} \exp\left(-\frac{(x - 2^j N_c \cos(\phi_x^w))^2}{2\sigma^2}\right) \exp\left(-\frac{(y - 2^j N_c \sin(\phi_x^w))^2}{2\sigma^2}\right). \tag{4.95}$$

The decorrelation properties of the DWT allows to assume the real and imaginary parts to be uncorrelated. The joint pdf of the amplitude r and phase θ, can be obtained by introducing the following equivalences $r = \sqrt{x^2 + y^2}$ and $\theta = \arctan(y/x)$. Hence

$$p_{r,\theta}(r,\theta) = \frac{r}{2\pi\sigma^2} \exp\left(-\frac{(r\cos(\theta) - 2^j N_c \cos(\phi_x^w))^2}{2\sigma^2}\right) \exp\left(-\frac{(r\sin(\theta) - 2^j N_c \sin(\phi_x^w))^2}{2\sigma^2}\right). \tag{4.96}$$

The pdf of the amplitude r is found by integrating Eq. (4.96) over θ

$$p_r(r) = \frac{r}{\sigma^2} \exp\left(-\frac{r^2 + 2^{2j} N_c^2}{2\sigma^2}\right) I_0\left(\frac{r 2^j N_c}{\sigma^2}\right) \quad r \in [0, \infty). \tag{4.97}$$

This pdf is known as Rice distribution after S. O. Rice derived it in the context of communication theory [71]. The shape of the Rice distribution is governed by the SNR ratio, which in this case has the expression $2^j N_c/\sigma$. For low values of SNR, the Rice distribution tends to a Rayleigh distribution, whereas for high values it tends to a Gaussian pdf, $\mathcal{N}(\mu, \sigma^2)$.

In the same way, the pdf of the phase can be found by integrating Eq. (4.96) over r. For simplicity reasons, ϕ_x^w is assumed to be equal to zero. Therefore

$$p_\theta(\theta) = \frac{1}{2\pi} \exp\left(-\frac{2^{2j} N_c^2}{2\sigma^2}\right) \left[1 + \frac{2^j N_c}{\sigma}\sqrt{\frac{\pi}{3}} \cos(\theta) \exp\left(\frac{2^{2j} N_c^2 \cos^2(\theta)}{2\sigma^2}\right) \left(1 + \operatorname{erf}\left(\frac{2^j N_c \cos(\theta)}{\sqrt{2}\sigma}\right)\right)\right]$$

$$\theta \in [-\pi, \pi) \tag{4.98}$$

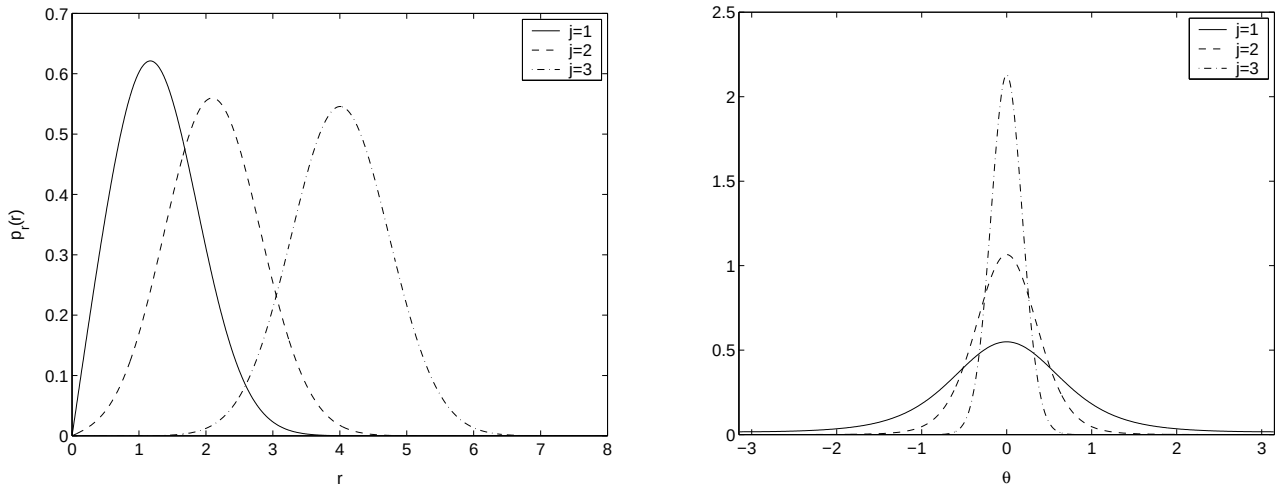

(a) (b)

Figure 4.18: Effect of the number of wavelet scales j over the wavelet coefficients distributions. In all the cases the quotient N_c/σ corresponds to a coherence equal to 0.6, which is approximately equal to 0.66. As observed, the larger the wavelet scale the higher the mean amplitude and the lower the phase noise content. (a) Amplitude distribution. (b) Phase distribution.

where erf(·) is called the error function[3]. This distribution is also controlled by the SNR ratio $2^j N_c/\sigma$ in such a way that for low SNR values $p_\theta(\theta)$ is close to a uniform distribution whereas for high values it is controlled by a Gaussian distribution.

This distribution model completely matches with the generalized noise model for the interferometric phasor at the wavelet domain, developed at Section 4.4. In those cases in which the coefficients contain useful information, that is $2^j N_c \neq 0$, the amplitude contains information about coherence (within the term N_c), whereas, the phase contains information about the wavelet interferometric phase ϕ_x^w. The higher the SNR ratio $2^j N_c/\sigma$, the lower the noise content both in amplitude and phase. The most important fact is that the SNR is controlled by the coherence value, by means of N_c/σ, but also by the factor 2^j which is introduced by the wavelet transformation process. At Fig. 4.18, one can observe the effect of the number of wavelet scales for a coherence equal to 0.6.

For SAR images from natural scenes, access to the original data is not possible as a consequence of speckle noise. Therefore, in order to test the statistical model which has been proposed, simulated interferometric phase images are employed. The method to synthesize these images has been already presented at Section 4.2.3. In this case, a simulated ramp producing 20-pixel fringes with a coherence $|\rho| = 0.6$ has been generated. A 3-scale DWT, calculated with 20-coefficient Daubechies filters, has been applied. In this case, useful signal appears concentrated on the coarse approximation band. Therefore, all the wavelet bands are only affected by noise. A Kolmogorov-Smirnov (KS) [178] test has been applied to test the Gaussian distribution of the wavelet coefficients real part. Also the kurtosis [178], as a measure of Gaussian behavior is included. Table 4.3 presents the results of this test. As it can be observed for all the wavelet bands, the significance levels for the KS test present high values. These results, together with the fact that in all the cases the kurtosis values are close to 3, confirm that these coefficients can be assumed to be described by a Gaussian pdf.

For the coarse approximation coefficients, the same analysis is applied. But, since in this case the coefficients contain the signal due to the interferometric phase ramp, a KS test under the assumption of a Rice distribution is applied. The significance level in this case corresponds to a value of $95,27\%$ with a kustosis equal to 3.08. This result confirms that the amplitude of those coefficients at the wavelet domain containing useful information are described by a Rice distribution.

[3]The error function is defined as $\mathrm{erf}(x) = \frac{2}{\sqrt{\pi}} \int_0^x \exp(-t^2)\,\mathrm{d}x$

	Horz. det. band (H)		Vert. det. band (V)		Diag. det. band (D)	
	Kurtosis	KS sig.lev.	Kurtosis	KS sig.lev.	Kurtosis	KS sig.lev.
Scale 2^1	2.98	87.93%	2.98	79.83%	2.94	98.34%
Scale 2^2	3.03	95.78%	2.97	86.08%	3.00	66.15%
Scale 2^3	3.08	82.87%	2.95	85.32%	3.00	82.87%

Table 4.3: Kurtosis and KS significance levels, under a Gaussian assumption, for the real part of the simulated complex interferometric phase ramp at the wavelet domain.

In this case, the distribution tests have been applied on the real part of the data. The same level of agreement is obtained for the imaginary part. Additional tests with different levels of coherence have also been performed. In all the cases, the KS tests have shown that the real and imaginary parts of the wavelet coefficients can be described by Gaussian distributions if they do not contain useful information, producing the amplitude to be rayleigh distributed. On the contrary, in those cases in which the coefficients contain useful information, the KS test have shown that intensity can be described by a Rice distribution. Finally, it can be concluded that the noise terms v_c^w and v_s^w can be considered to be Gaussian distributed noises, $\mathcal{N}(0, \sigma^2_{v_c^w})$ and $\mathcal{N}(0, \sigma^2_{v_s^w})$ respectively.

The topographic model assumed previously (i.e.: constant slope) does not take into account spatial details, which are important, for instance, in urban areas. As no information is available about the distribution of the topographic phase ϕ_x, an a priori model for the spatial details is not available in the spatial domain. This drawback can be overcome in the wavelet domain. As mentioned before, the DWT can be interpreted as a weighted sum of random variables. Therefore, $DWT_{2D}\left\{N_c \cos\left(\phi_x\right)\right\}$ and $DWT_{2D}\left\{N_c \sin\left(\phi_x\right)\right\}$ can be supposed to be determined, as a first approximation, by a Gaussian pdf. Test with real InSAR data show clear deviations from this behavior [177]. To take into account this deviation from gaussian behavior, a double stochastic model is proposed for the wavelet coefficients x

$$p_x\left(x\right) = \int_0^\infty p_x\left(x|_{\sigma^2}\right) p_{\sigma^2}\left(\sigma^2\right)\, \mathrm{d}\sigma^2 \tag{4.99}$$

where $p_x\left(x|_{\sigma^2}\right)$ represents the gaussian distribution of the wavelet coefficients and $p_{\sigma^2}\left(\sigma^2\right)$ is a generalized gamma pdf modelling the variability of the variance through the phase image. $p_x\left(x\right)$ can not be obtained in a general form. Numerical integration of (4.99) indicates that $p_x\left(x\right)$ can be assumed to be a generalized gaussian pdf [177].

4.6 A Study Case: Mt. Etna (Italy)

As it has been presented throughout the development at the previous sections, it has been possible to define a new noise model for the interferometric phasor in the wavelet domain. The availability of such a noise model has allowed to derive diverse results, among which it is important to underline the potential offered by the wavelet analysis theory to extract relevant interferometric information in the wavelet domain.

The present section concerns the study of this set of results by employing a real interferometric phase image. The phase image corresponds to a 512 by 512 pixel, X-band interferogram of Mt. Etna (Italy) taken by the E-SAR system which is operated by the German Aerospace Center (DLR). The corresponding interferometric phase can be observed at Fig. 4.19a. The phase image can be divided in three main regions. The upper right-hand corner corresponds to a medium to high coherence area with a given slope. The middle region contains a steeper topography with lower coherence. Finally, the down left-hand corner corresponds to a shadow area, therefore only noise is present. In this case the coherence is approximately zero as it can be seen at the coherence image, Fig. 4.19b. The DWT has been applied to the interferometric phasor obtained from the interferometric phase of Mt. Etna. In this case, the depth of the DWT corresponds to three wavelet scales, i.e.: $2^j = 2^3$, since noise effects are negligible in

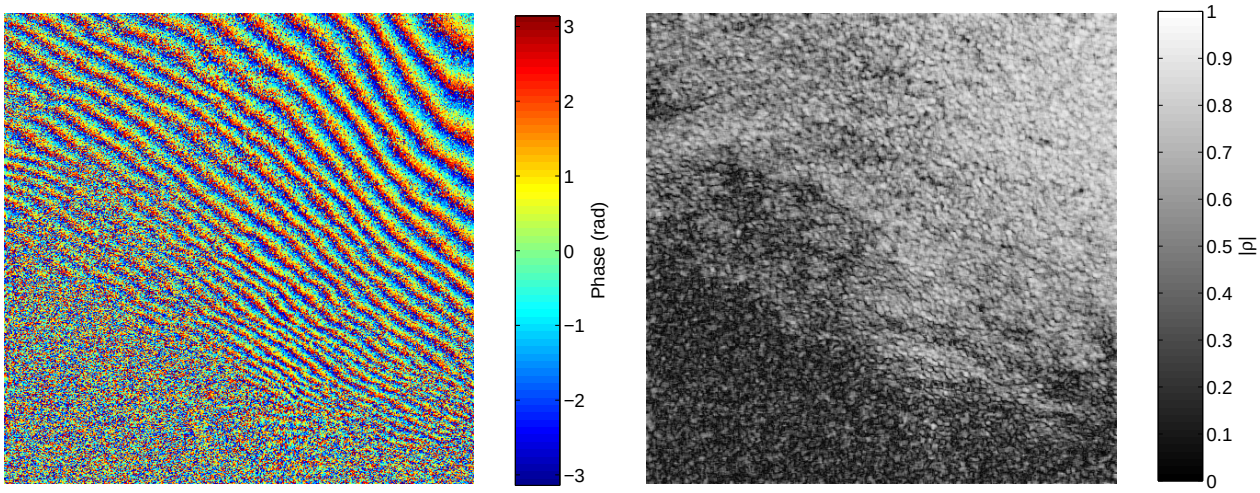

(a) (b)

Figure 4.19: Mt. Etna Interferogram. (a) Phase. (b) Coherence.

the intensity of the wavelet coefficients. A 10 coefficient Daubechies filters have been employed to obtain the DWT. Fig. 4.20 presents the different results in the wavelet domain. The first column corresponds to the complete signal in the wavelet domain, whereas the second one corresponds to a zoom of the third wavelet scale, which are from left to right and from top to bottom the bands $a_3[m,n]$, $d_3^H[m,n]$, $d_3^V[m,n]$ and $d_3^D[m,n]$. The first row contains the values of the real part of the coefficients, the second one corresponds to the amplitude and the third one contains the phase of the wavelet coefficients.

At a first sight, it can be observed that useful information is concentrated on the lower frequency wavelet bands, where it can be seen that the real part coefficients present larger values. This effect is evident on the amplitude images, Figs. 4.20c and 4.20d. As it has been demonstrated theoretically, it can be seen that intensity contains coherence information, whereas the corresponding phase information is very similar to the original interferometric phase. From Fig. 4.20f, it can be seen that the coarse approximation coefficients phase is proportional to the original interferometric phase. The middle part of the interferometric phase image appears on the wavelet band $d_3^V[m,n]$, since it presents an steeper slope which has the largest Wavenumber Shift at the whole image. The corresponding amplitude presents large values confirming that the useful information at the wavelet domain has to be understood as a modulated coherence. The phase information, in this case, does not correspond to the original interferometric phase as a consequence of the downsampling and frequency inversion of a band-pass signal. Finally, those wavelet coefficients which do not depend on the useful signal component present low intensities values and the phase does not contain information at all.

Of special importance is the fact that it is possible to derive coherence information in the wavelet domain, through the amplitude of the wavelet coefficients. If the original coherence presented in Fig. 4.19b is compared with the amplitude information in the wavelet domain given by Figs. 4.20c and 4.20d, one can observe the similarity between both quantities. For the wavelet images case, amplitude corresponds to a division of the original coherence in a space-frequency frame, where the position in the wavelet scale dimension is controlled by the interferometric phase.

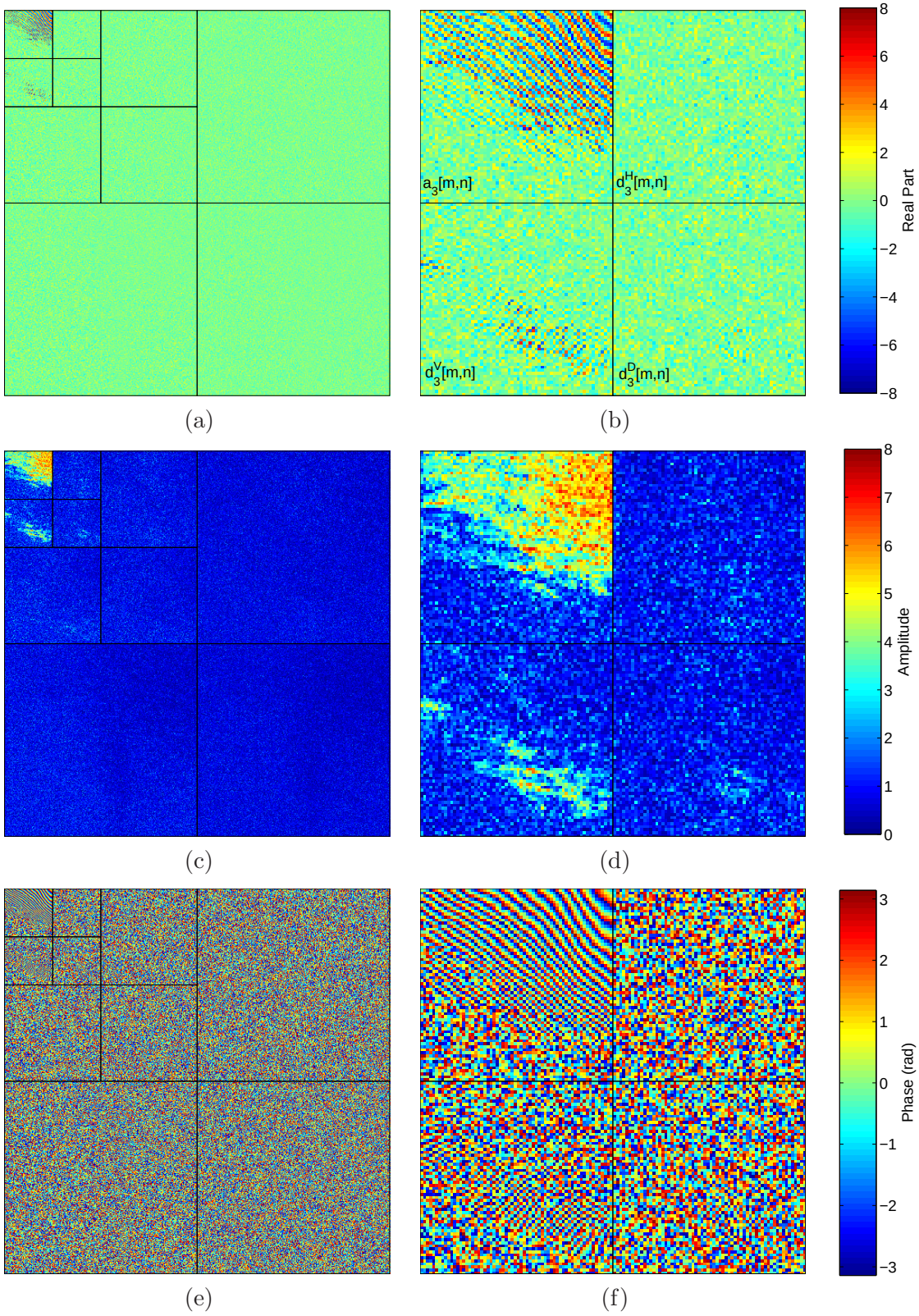

Figure 4.20: DWT of the interferometric phasor corresponding to the Mt. Etna data. The DWT consists of three transformed scales calculated with the Daubechies wavelet filter of the coefficients. (a) DWT of the interferometric phasor's real part, $\Re\{DWT_{2D}\{e^{j\phi}\}\}$. (b) Zoom corresponding to the third wavelet scale. (c) Wavelet coefficients amplitude, $|DWT_{2D}\{e^{j\phi_x w}\}|$. (d) Zoom corresponding to the third wavelet scale. (e) Wavelet interferometric phase $\arg\left\{DWT_{2D}\{e^{j\phi}\}\right\}$. (f) Zoom corresponding to the third wavelet scale.

4.7 Summary

This chapter concerns the study, analysis and validation of a noise model for the interferometric phasor, that is, the unit amplitude phasor whose argument consists in the interferometric phase difference, both, in the original and in the wavelet domain.

The interferometric phase additive noise model in the real plane, as a result of the Gaussian scattering assumption, permits to separate, in the complex plane, useful information from those terms which contain only noise. The detailed analysis of the probability density functions associated with the interferometric phasor has allowed to establish a novel noise model for this phasor. The useful information term, which has been defined as the modulated coherence term, contains the true interferometric phase, but also the interferometric coherence information through the parameter N_c. This useful term is damaged by a complex additive noise term, whose real and imaginary parts have a mean equal to zero and a variance which decreases with increasing coherences. The noise model is tested quantitatively with simulated and real interferometric SAR data. Finally, the validity of the model has been extended to multilook interferometric SAR data.

Since interferometric SAR data are characterized by a high spatial resolution, it is necessary to remove phase noise without destroying this important property. As explained in Chapter 1, the wavelet analysis theory is employed as the mathematical tool to perform this task. Consequently, in order to derive an optimum noise reduction algorithm, but also, to understand how the useful information is divided in the wavelet domain, the interferometric phasor noise model has been translated to this new domain. The process to obtain this model has made necessary to idealize both: the signal to transform and the discrete wavelet transform itself. On the basis of these idealizations, it has been demonstrated that the amplitude of the complex wavelet coefficients is basically determined by the interferometric coherence, whereas the phase depends on the interferometric phase. The most important result is to prove that the wavelet transform itself can be considered as a interferometric phase filter. This filtering process is obtained at the expense of spatial resolution, but the relevant issue is that this spatial resolution loss can be recovered in the inverse transformation process. Therefore, this loss does not represent a main drawback. This improving effect introduced by the discrete wavelet transform, proved through the noise model, has been ratified by the fact that the complex wavelet coefficient are described by a Rice probability density distribution, when only topography is considered.

This set of new noise models have been derived on the basis of the interferometric phase signal to contain only a well defined topography. This is not the case for real interferometric phases due to the phase image details, which can not be modelled efficiently, since they represent a very heterogeneous component. As it will be demonstrated in subsequent chapters, the wavelet transform's capability to represent these details makes not necessary to model them. One can conclude that the wavelet analysis theory itself permits to bridge the gap between what the interferometric phase noise model represents and what the real interferometric signal contains.